Large-cell Monte Carlo renormalization group for percolation*

Peter J. Reynolds, H. Eugene Stanley, and W. Klein
Department of Physics and Center for Polymer Studies, Boston University, Boston, Massachusetts 02215
(Received 13 August 1979)

We obtain the critical parameters for the site-percolation problem on the square lattice to a high degree of accuracy (comparable to that of series expansions) by using a Monte Carlo position-space renormalization-group procedure directly on the site-occupation probability. Our method involves calculating recursion relations using progressively larger lattice rescalings, b. We find smooth sequences for the value of the critical percolation concentration $p_c(b)$ and for the scaling powers $y_p(b)$ and $y_h(b)$. Extrapolating these sequences to the limit $b \to \infty$ leads to quite accurate numerical predictions. Further, by considering other weight functions or "rules" which also embody the essential connectivity feature of percolation, we find that the numerical results in the infinite-cell limit are in fact "rule independent." However, the actual fashion in which this limit is approached *does* depend upon the rule chosen. A connection between extrapolation of our renormalization-group results and finite-size scaling is made. Furthermore, the usual finite-size scaling arguments lead to independent estimates of p_c and y_p. Combining both the large-cell approach and the finite-size scaling results, we obtain $y_p = 0.7385 \pm 0.0080$ and $y_h = 1.898 \pm 0.003$. Thus we find $\alpha_p = -0.708 \pm 0.030$, $\beta_p = 0.138(+0.006, -0.005)$, $\gamma_p = 2.432 \pm 0.035$, $\delta_p = 18.6 \pm 0.6$, $\nu_p = 1.354 \pm 0.015$, and $2 - \eta_p = 1.796 \pm 0.006$. The site-percolation threshold is found for the square lattice at $p_c = 0.5931 \pm 0.0006$. We note that our calculated value of ν_p is in considerably better agreement with the proposal of Klein *et al.* that $\nu_p = \ln\sqrt{3}/\ln(\frac{3}{2}) \cong 1.3548$, than with den Nijs' recent conjecture, which predicts $\nu_p = \frac{4}{3}$. However, our results cannot entirely rule out the latter possibility.

I. INTRODUCTION

The recently much-studied percolation problem, which deals with the cluster properties of a system, is a mathematical problem of great interest in itself.[1] However, it is also a model of much utility in describing many physical situations, ranging from dilute magnets,[2] cluster properties of the Ising model,[3] conduction in random systems,[4] and polymer gelation,[5] to fluid flow through porous materials.[6] For general reviews of some of these problems, and for further references, see Refs. 7 and 8.

In the "pure" percolation problem, the elements (usually taken to be sites or bonds on a lattice) are placed entirely at random. Although this is a model of a *noninteracting* system, it is intriguing that it nevertheless exhibits critical behavior. The singularities in the percolation problem occur in the properties of the physical clusters, rather than in quantities related to the thermodynamic properties, such as the net fraction of sites that are occupied. This latter quantity, the magnetization, might also have a singularity in an interacting system—though as a function of the thermodynamic variables. The study of a critical phenomena has most commonly concerned itself with such thermodynamic quantities. However, the critical point that occurs in pure percolation is remarkably similar to critical points in interacting systems. In fact, particular limits of interacting systems (describable by Hamiltonians) reduce to pure percolation (which is entirely statistical, and has no Hamiltonian).

In particular, the $s \to 1$ limit[9] of the s-state Potts model[10] corresponds to pure bond percolation. This fact provided the initial bridge between conventional critical phenomena and percolation. The vast arsenal of theoretical tools available for studying cooperative phenomena was soon employed to study this limit. In particular, the renormalization group[11] was applied to the Potts Hamiltonian both in momentum space by ϵ expansion from $d = 6$ dimensions[12,13] and in real space.[12,14] However, a Hamiltonian is not necessary for studying percolation. The existence of a diverging length scale is sufficient to motivate the use of the renormalization group. Young and Stinchcombe[15] showed how a decimation procedure applied directly on the bond occupation probabilities—in which a set of vertices is summed over, leading to renormalized bond probabilities on a rescaled lattice—is equivalent to summing out degrees of freedom in the Potts partition function. Furthermore, Kirkpatrick[16] used Migdal recursion relations[17] directly on the probabilities, again for the bond problem.

The present authors were able to treat *both* site and bond percolation using a Niemeijer–van Leeuwen-type cluster approach directly on the occupation pro-

babilities.[18] We chose a renormalization transformation which reflects the fact that the order parameter in percolation is the fraction of occupied sites in a percolated (infinite) cluster, rather than the net number of sites occupied. The transformation embodies the "connectivity rule": a block "spin" is taken to be occupied if the "spins" of which it consists form a *spanning cluster*. This reflects the fact that the singularities occur in the cluster properties. A majority-rule transformation, such as is used for the Ising model, has a symmetry which picks out singularities in the magnetization. We showed that the procedure of block renormalization is exact in one dimension ($d=1$), though in higher dimensions approximations are necessary. Results for small cells on various lattices were encouraging. In the same paper we also showed how a ghost site[9,19] could be introduced to directly rescale a field probabililty. In that way we were able to calculate the field scaling power as well as the "thermal" (occupation probability) scaling power for $d=1$. Previous work[15,16] with direct rescaling of the probabilities had only dealt with the thermal scaling power.

Subsequently, Marland and Stinchcombe[20] performed a direct rescaling of the field in $d=1,2$ by a decimation transformation. An inherent flaw in their procedure (decimation implies $y_h=d$ or $\eta=2-d$) was subsequently circumvented by Marland by use of a variational technique.[21] Also, Yuge[22] has calculated the thermal exponents (though not the field exponents) for various $d=2$ cells on a number of lattices, using a block formulation similar to our original one. Kunz and Payandeh[23] have also used this type of block transformation to calculate both thermal and field scaling powers for small cells in $d=2,3$. Tsallis and Schwachheim[24] have defined several alternative transformations for the occupation probability, and catagorized the types of "rules" for percolating. Further work with direct rescaling[25–28] has included the conductivity problem,[26] site-bond percolation,[27] and calculation of cluster numbers.[28] Also, we introduced the use of very large cells for percolation and reported preliminary results for site percolation.[29] Here our discussion goes into greater depth, and we treat extensions of that early work. The large-cell method has also recently been followed by Kirkpatrick[8] and Magalhães *et al.*[30] for bond percolation.

We begin in Sec. II with some preliminaries on position-space renormalization group (PSRG) for percolation. Then, in Sec. III we give examples of calculations with small cells. We discuss why we expect improvement in our results with increasing cell size. In order to proceed with large-cell calculations, the definitions and properties of our rescaling transformations are given in Sec. IV. All these renormalization rules embody the physics of percolation via connectivity. We then show how we calculate the closed-form and Monte Carlo recursion relations using these connectivity weight functions. In Sec. V we present the results obtained by applying these connectivity weight functions to cells of size up to 250 000 sites. In this way we obtain sequences for the values of the percolation threshold p_c and for the scaling powers y_p and y_h from which all the critical exponents may be obtained. We also show how extrapolation of these sequences to the limit of infinite cell size leads to quite accurate numerical results. For our connectivity weight functions, we find that these numerical results are in fact "rule independent". How rapidly we converge to this limit, however, does depend upon the rule chosen. We also discuss connections with finite-size scaling. In Sec. VI we discuss our results. In particular, our calculation of y_p may be considered a test of the recent conjecture of den Nijs,[31] which connects the s-state Potts model to the eight-vertex model. We find that den Nijs' value for $s=1$ (percolation) does not agree as well with our results as the value of y_p proposed by Klein *et al.*,[32] though den Nijs' result cannot be entirely ruled out by our calculations. Appendix A presents the closed-form PSRG calculation of the $d=1$ percolation problem with further-neighbor bonds. We derive the recursion relations for arbitrary rescaling length b, and show that in the limit $b\to\infty$ we obtain the exact results known for this model.[33]

II. POSITION-SPACE RENORMALIZATION GROUP FOR PERCOLATION

In the Niemeijer–van Leeuwen approach to the position-space renormalization group,[11] one starts by partitioning a lattice into cells which both cover the lattice and which—if viewed from a perspective in which these cells are renormalized sites—form a lattice which has precisely the same symmetry as the original. One thing has changed, however, and that is the length scale. Measured in terms of the new lattice constant, all distances are smaller by a factor of $b=N^{1/d}$, where N is the number of sites in a cell, and d is the dimension of the space. If on the renormalized lattice the functions of interest are to maintain the original singularity structure, these functions must have the same form as before (assuming we keep the same number of arguments). These arguments (the "coupling constants") must now be at new renormalized values, however, to compensate for the change in length scale.

To illustrate the above, consider ξ_p, the analog of the correlation length in thermal critical phenomena. In percolation this is the connectedness length, which is a measure of a typical linear cluster dimension—the rms cluster diameter for example. On the renormalized lattice ξ_p is smaller by a factor of b, and thus we are further from criticality (at which point ξ_p diverges). This is reflected, for example, in the site occupation probability p, which is renormalized to a

value further from the percolation threshold p_c.

If we let $\{p_i\}$ denote the set of occupation probabilities of various kinds (sites, nearest-neighbor bonds, further-neighbor bonds, and so forth) then all the coupling constants in $\{p_i\}$ will be renormalized, as we shall see below. Thus, we may write

$$\xi_p(\{p_i'\}) = \frac{1}{b}\xi_p(\{p_i\}) \quad . \tag{2.1}$$

It is the basis of the cluster approximation to consider a small cluster of neighboring cells, and to renormalize only those members of $\{p_i\}$ that "fit" into the cluster. This procedure, however, involves an approximation because the renormalized occupied sites created in this process have connectivity functions (e.g., the pair connectedness) that differ from those on the original lattice of randomly occupied sites. A cluster containing more than one cell thus necessitates the introduction of additional probabilities from $\{p_i\}$ into the equation for the renormalized p' (and these additional probabilities are in fact themselves renormalized). These new couplings are used to "undo" the unwanted connectivity correlations.

The result of all this is a renormalization-group transformation

$$\{p_i'\} = R(\{p_i\}) \quad . \tag{2.2}$$

This transformation has a "fixed point" where R leaves the coupling-constant space unchanged: $\{p_i^*\} = R(\{p_i^*\})$. By Eq. (2.1) we see that physically a fixed point corresponds to either $\xi_p = 0$ or $\xi_p = \infty$, and thus the critical point, at which $\xi_p = \infty$, is to be associated with a fixed point of Eq. (2.2). However, a complete and exact treatment in this manner would involve an infinite number of coupling constants p_i, and a cluster of cells covering ever larger regions of the lattice. Equation (2.2) would then become an infinite set of coupled equations. Somewhere we must truncate.

This paper treats the truncation induced by considering the one-cell cluster. As we will discuss in Sec. III, the severity of the unwanted correlation introduced by renormalization appears to diminish with the size of the single cell. Thus the approximation improves progressively with increasing cell size. Our results can, in fact, be extrapolated to the limit of infinite cell size, where the single-cell cluster possibly becomes exact.[34] For the case of the single cell, the only probabilities in the set $\{p_i\}$ that enter are p, the site occupation probability, and h, the "ghost"-bond occupation probability.[9,19,35] The ghost-field bonds are physical links from a single "ghost site" which is not on the lattice to each site on the lattice. If one were to quantify the cluster properties by their bond size rather than by their site size, the ghost bonds would link to every bond in the lattice instead.[35] Such ghost bonds drastically change the topology of the lattice when $h \neq 0$, causing many finite clusters to be connected to a single infinite cluster. The ordinary percolation threshold obtains when $h = 0$.

In order to obtain the critical properties for percolation in this approximation, we must calculate the recursion relations

$$p' = R_p(p,h) \tag{2.3a}$$

and

$$h' = \tilde{R}_h(p,h) \quad . \tag{2.3b}$$

The percolation threshold corresponds to a fixed point at $(p^* = p,\ h^* = 0)$. In practice $h^* = 0$ is readily obtained, since Eq. (2.3b) may be written

$$h' = hR_h(p,h) \quad , \tag{2.4}$$

with $R_h(p,0)$ finite.[36] Thus we decouple the two recursion relations immediately by evaluating p' as a function of p alone. Then, by calculating the eigenvalues of the renormalization-group transformation linearized about the fixed point, we obtain the necessary information for calculating the critical-point exponents. Briefly, this is done in the following way:

The average of the *total number* of clusters on the lattice, upon renormalization, should remain constant up to a nonsingular term.[32,37] Thus we may relate the singular part of the average number of clusters, G_s (now taken per site) before and after renormalization by

$$G_s((p'-p^*),h') = b^d G_s((p-p^*),h) \quad , \tag{2.5}$$

since the new lattice contains a factor of b^d fewer sites than the original lattice.

Very near the fixed point we may linearize the decoupled renormalization-group equations (2.3) to obtain[36]

$$(p'-p^*) = \lambda_p(p-p^*) \quad , \tag{2.6a}$$

$$h' = \lambda_h h \quad , \tag{2.6b}$$

with

$$\lambda_p = \left.\frac{dp'}{dp}\right|_{\substack{p=p^* \\ h=0}} \tag{2.7a}$$

and

$$\lambda_h = \left.\frac{dh'}{dh}\right|_{\substack{p=p^* \\ h=0}} \quad . \tag{2.7b}$$

Defining the scaling powers y_x by

$$\lambda_x \equiv b^{y_x} \quad , \tag{2.8}$$

we may rewrite Eq. (2.5) as [cf. Eq. (2.6)]

$$G_s(b^{y_p}(p-p^*), b^{y_h}h) = b^d G_s(p-p^*,h) \quad . \tag{2.9}$$

All the usual percolation exponents may be determined in terms of y_p and y_h. This is because the singular part of all the "thermodynamic" percolation functions may be obtained by taking appropriate derivatives of Eq. (2.9).[35] For example, the singular behavior of the "Gibbs potential," or the mean total number of clusters, is given by

$$G_s(p,h=0) \sim |p-p^*|^{2-\alpha_p} \ . \tag{2.10a}$$

The "order parameter", the fraction of occupied sites belonging to the infinite cluster, varies as

$$P(p,h=0) \sim \frac{\partial G_s(p,h)}{\partial h}\bigg|_{h=0} \sim (p-p^*)^{\beta_p} \tag{2.10b}$$

and

$$P(p=p^*,h) \sim \frac{\partial G_s(p^*,h)}{\partial h} \sim h^{1/\delta_p} \ . \tag{2.10c}$$

The "susceptibility", which is the mean cluster size, diverges as

$$S(p,h=0) \sim \frac{\partial^2 G_s(p,h)}{\partial h^2}\bigg|_{h=0} \sim |p-p^*|^{-\gamma_p} \ . \tag{2.10d}$$

From the generalized homogeneous function form of Eq. (2.9) it follows that[38]

$$2-\alpha_p = d/y_p \ , \tag{2.11a}$$

$$\beta_p = (d-y_h)/y_p \ , \tag{2.11b}$$

$$\delta_p^{-1} = (d-y_h)/y_h \ , \tag{2.11c}$$

and

$$\gamma_p = (2y_h - d)/y_p \ . \tag{2.11d}$$

The "correlation function" exponents may also be derived from y_p and y_h as follows. Near the fixed point, the connectedness length ξ_p diverges as

$$\xi_p \sim |p-p^*|^{-\nu_p} \ . \tag{2.12}$$

Combining Eqs. (2.6a) and (2.8) we have

$$(p'-p^*) = b^{y_p}(p-p^*) \ . \tag{2.13}$$

It follows on raising Eq. (2.13) to the $(-\nu_p)$ power, that $\xi_p' = b^{-y_p\nu_p}\xi_p$. Comparing this with Eq. (2.1) we find

$$\nu_p = y_p^{-1} \ . \tag{2.14}$$

Furthermore, it is readily shown from scaling[38] that, by integrating $C_2(r)$ to obtain $S(p)$, $\gamma_p/\nu_p = 2-\eta_p$. Hence

$$2-\eta_p = 2y_h - d \ . \tag{2.15}$$

III. SMALL CELLS VERSUS LARGE CELLS

A. Calculations with small cells

We will now make our discussion concrete with a few examples. We begin by discussing small cells on various lattices. At this point, our concern is only with renormalizing the occupation probability p, at $h=0$. Thus the first step is to find the function $R_p(p,h=0)$ of Eq. (2.3). The renormalization transformation must reflect the fact that percolation involves the formation of an infinite connected network—that is, one that actually "gets across" the entire lattice. Below the percolation threshold only finite clusters are present. Thus we define a cell as occupied if and only if it contains a set of sites such that the cell "percolates".[18] This determines $R_p(p,h)$ for us. Different possible definitions for when a finite cell has percolated are considered in Refs. 18 and 22–24, and Sec. IV of this paper. References 24, 29, and this paper discuss the effect of such choices of rule.

We demonstrate our approach first in one case where the transformation is exact. For the $d=1$ linear-chain lattice we define an l-site cell as occupied if we can get across it. This requires that all the sites be present. Thus[18]

$$p' = R_p(p,h=0) = p^l \ . \tag{3.1}$$

Setting $p'=p$, we find fixed points at $p^*=0,1$. The unstable fixed point at $p^*=1$ determines p_c. From Eq. (2.7a) we find $\lambda_p = l$. Since the rescaling length is $b=l$, Eqs. (2.8) and (2.14) yield $y_p=1$ and $\nu_p=1$, respectively. These are in fact the exact results.[35]

For $d=2$ the simplest cell is the three-site cell on the triangular lattice. Applying our rule, the cell is occupied if all three sites are occupied or if any two sites are occupied and one is vacant, since in both cases we can get across. However, with one or no sites the cell is vacant. Thus,[18]

$$p' = R_p(p,h=0) = p^3 + 3p^2(1-p) \ , \tag{3.2}$$

with fixed points at $p^*=0$, 1, and $\frac{1}{2}$. This PSRG therefore predicts $p_c = \frac{1}{2}$ for the triangular lattice, which is in argeement with the exact results known for this lattice.[1] Once again, from Eqs. (2.7a), (8), and (14), we calculate ν_p,

$$\nu_p = \ln\sqrt{3}/\ln(\tfrac{3}{2}) = 1.354\,7\cdots \ , \tag{3.3}$$

which is in excellent agreement with the series results $\nu_p = 1.34 \pm 0.02$ for the bond problem,[39] and $\nu_p = 1.32^{+0.02}_{-0.07}$ for the site problem.[40] Furthermore, Eq. (3.3) may be an exact result.[32] Others,[31] however, have proposed that $\nu_p = \frac{4}{3}$ exactly. We will return to this point in Sec. VI. Applying our transformation to the square lattice with a length rescaling factor of $b=2$, our results are not nearly as good. In particu-

lar we found[18] $\nu_p \simeq 1.64$, about 20% larger than the series result.

For bond percolation it is not as obvious how to choose a cell that covers the lattice with bonds, and rescales to another bond. We choose a simple eight-bond cell on the square lattice [see Fig. 3(a) of Ref. 18]. If the cell can be traversed horizontally, then the renormalized horizontal bond is present, and similarly for the vertical direction. We find[18]

$$R_p(p,h=0) = p^5 + 5p^4(1-p) + 8p^3(1-p)^2 + 2p^2(1-p)^3 \ , \tag{3.4}$$

with $p^* = 0.5$ (exact) and $\nu_p \simeq 1.43$. The generalization of this simple cell to the cubic lattice gives $p^* \simeq 0.21$ and $\nu_p \simeq 1.03$, while numerical work predicts[8] $p_c = 0.2495 \pm 0.0005$ and $\nu_p = 0.845 \pm 0.015$.

However, these $d > 1$ calculations all share one negative feature. They are single-shot calculations, whose approximation are uncontrolled. What is the nature of this approximation?

B. The approximation: Why large cells

As a natural beginning, we have treated the lowest-order approximation, using just a single cell in our cluster. Thus, we require only one lattice probability p together with a field h. Further, because the Eqs. (2.3) decouple, we are able to treat the probability p alone, as we have done in Sec. III A.

We have assumed that the renormalized sites are still random. Actually, the cells are not independent, and additional coupling constants need to be introduced to cancel this correlation effect. However, finding a solution to the coupled Eq. (2.2) becomes difficult when there are more than just a few elements in $\{p_i\}$.

As an alternative to this approach of increasing the space of coupling constants, we have retained the single-cell cluster. However, this simple PSRG, which might at first seem a poor approximation, may be systematically improved by treating successively *larger* cells.

In this single- or independent-cell approximation, the connectivity within a cell (the volume) is treated exactly. The approximation comes in at the interfaces *between* cells, where, upon renormalization, we lose some actual connecting paths, and gain other, new, connecting paths. In Fig. 1 we see an example of the problems encountered at the interface between cells.

We note that with increasing cell size, the interfacing problem plays a progressively smaller role, as it is a surface effect (edge of a cell), whereas the connectivity within a cell involves the full cell volume. While these surface effects vanish as b tends to infinity, the treatment of the ever-enlarging interior volume remains exact. Thus, intuitively we would

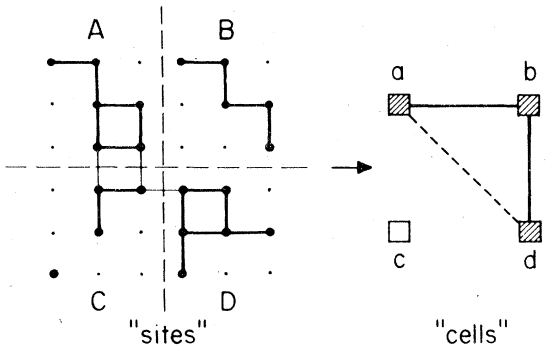

FIG. 1. Illustration of the interfacing problem between cells. Cells A, B, and D are each connected from edge to edge, and, by the connectivity rule described in the text, occupied upon renormalization ("cell sites" a, b, and d). Two competing effects are illustrated: (i) A and B do not join (by nearest-neighbor bonds alone) on the site level, yet a and b are joined implicitly at the cell level. The introduction of a new member of the set $\{p_i\}$, $p_{\rm nn}$, would solve this problem where $p_{\rm nn}$, the probability of a nearest-neighbor *bond* being occupied, would no longer be constrained to unity (Ref. 27). (ii) A and D *are* joined through nearest-neighbor bonds on the site level. On the cell level a and d ought to be joined; however c is empty. Another member of $\{p_i\}$, $p_{\rm nnn}$, the probability of a next-nearest-neighbor bond being occupied, would now be needed if we were to follow this approach. Both these effects may be overcome by either introducing additional members of $\{p_i\}$, or by going to larger cells. In the example pictured here, $b = 3$.

expect the approximation to become better as the cell size increases. This is indeed borne out, as we will see in Sec. V.

An illustration of how this surface effect becomes negligible is given in Fig. 2. Let X_I be the average fraction of sites belonging to the spanning cluster of cell I. The probability that two such spanning clusters do *not* join at one point on the interface is $(1 - X_A X_B)$. If the sites belonging to the spanning cluster were independently distributed—which strictly speaking they are not—we could write the probability that the two spanning clusters touch nowhere along the interface as $(1 - X_A X_B)^{b^{(d-1)}}$, where $b^{(d-1)}$ is the number of sites at which cells A and B meet. As long as $X_A \neq 0$, $X_B \neq 0$ (i.e., the two cells each contain a spanning cluster, and are therefore "occupied"), we find[41]

$$\lim_{b \to \infty} (1 - X_A X_B)^{b^{(d-1)}} = 0 \ . \tag{3.5}$$

Such a form implies that, as the cell size tends to infinity, there is no chance that two occupied cells do not link together. We expect a form similar to this to hold true, even though the sites in the spanning cluster are not independent.

Likewise, the probability of having two occupied, diagonally opposite, cells (e.g., cells A and D of

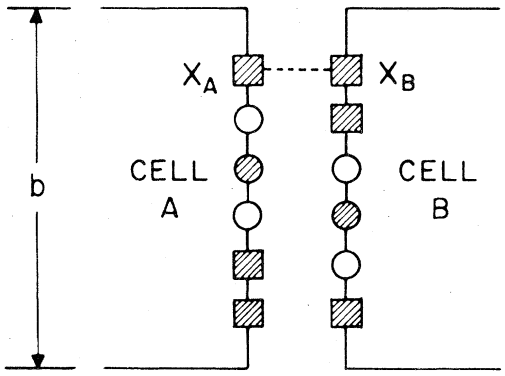

FIG. 2. Interfacing problem diminishes with increasing cell edge, b. It is likely that the probability of two occupied nearest-neighbor cells not linking vanishes as $b \to \infty$. A discussion of why this might be is given in the text. A particular realization is shown here, with sites belonging to the spanning clusters drawn as shaded squares, and occupied sites (not part of the spanning clusters) drawn as shaded circles. Open circles represent empty sites.

Fig. 1) connected through an empty cell (e.g., C) vanishes as $b \to \infty$. This is so because at large b, and at a value of p high enough that A and D are occupied, a cluster in C sufficiently branched to connect to both the spanning clusters in A and D will tend also to be branched enough to span C. This effect increases as $b \to \infty$ because, on the average, larger clusters will be needed to connect A to D, and these are more likely to span C.

We have argued that the surface effects diminish as we increase b. In addition, our PSRG transformation treats the interior connectivity correctly for all b. To see that the volume is treated properly, and that the rescaling transformation (of getting across) makes sense, consider an infinite cell. The cell now comprises the whole lattice. Since the renormalized site-occupation probability p' is the probability of spanning the lattice, we find $p'=0$ if $p < p_c$, and $p'=1$ if $p > p_c$. Thus $p'=p=p^*$ at $p=p_c$. The transformation (if we could determine it for an infinite lattice) produces the exact p_c. Although the transformation $R_p(p,h)$ is itself singular when $b=\infty$, we will treat finite values of b and extrapolate the results to the limit $b \to \infty$.

A further reason why we expect this limit to be correct stems from our PSRG treatment of percolation on the linear-chain lattice with further-neighbor bonds (cf. Appendix A). Here the exact result for ν_p obtains in the limit of the cell size tending to infinity.

IV. CALCULATION OF CLOSED-FORM AND MONTE CARLO RECURSION RELATIONS

In this section we will be dealing with the PSRG equations obtained by using the two coupling constants p, the site occupation probability, and h the probability of a ghost bond. We will study the transformations

$$p' = R_p(b:p,h) \tag{4.1a}$$

and

$$h' = hR_h(b:p,h) \ , \tag{4.1b}$$

both for their general properties, and specifically for methods to calculate them for various values of the rescaling length b. Calculation of these recursion relations, however, involves first defining the above two transformations, R_i.

A. Definition of the rescaling transformations

On physical grounds R_p is any cell-to-site transformation which uses connectivity of the cell as the determining factor for a renormalized site being occupied. We have defined three such "rules" for the square lattice, though they apply equally well to other lattices with "square-like" cells (e.g., four-site, nine-site, ..., b^d-site cells on the triangular or square matching lattices). These rules state that a cell is occupied if and only if there is a spanning cluster[43] in the cell, which, for rule R_0: spans the cell *either* horizontally or vertically; R_1: spans the cell in a *fixed* direction (e.g., horizontally); or R_2: spans the cell *both* horizontally and vertically.

These rules are not independent of one another, as we may, for example, calculate $R_0(p,h)$ as the probability of spanning horizontally *plus* the probability of spanning vertically, *minus* any over-counting of clusters that span horizontally and vertically. Thus,

$$R_0(p,h) = 2R_1(p,h) - R_2(p,h) \ . \tag{4.2}$$

As a result, it is sufficient to study only two of these three rules in detail. We will consider primarily R_0 and R_1.

Furthermore, at $h=0$, these functions obey matching relationships

$$R_1(p) + R_1^M(q) = 1 \tag{4.3a}$$

and

$$R_2(p) + R_0^M(q) = 1 \ , \tag{4.3b}$$

where $q=1-p$, and the M means that the rule is to be applied to the matching graph of the original cell, and hence to a study of the matching lattice[44] (see Fig. 3).

We may understand Eq. (4.3a) by considering each configuration of occupied ("black") and vacant ("white") sites: if we can span the cell horizontally with black sites, then they form a blockade on the matching lattice for a vertical path by white sites [see Fig. 3(a)]; if there is no black path horizontally, there is always a vertical path with white sites on the

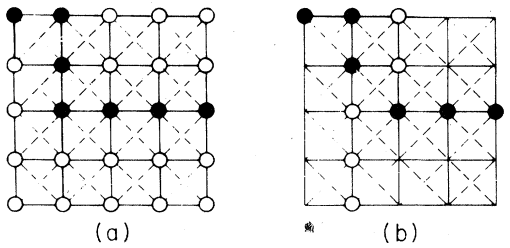

FIG. 3. Configurations of two species of sites, blacks (solid circles) and whites (open circles), on a 5×5 cell. Solid lines represent bonds on the square lattice, L. Dashed lines are additional bonds which are present in the square matching lattice, L^M. In (a), a horizontal spanning path of black sites (in this case spanning both L and L^M) blocks any vertical path by white sites on the matching lattice (either L^M or L). Part (b) shows part of a configuration, where blacks do not span horizontally on L, but whites do span vertically on L^M. Note, it we were to interchange L and L^M, there *is* a horizontal path of blacks, but now there is no longer a vertical path of whites on L^M.

matching lattice [see Fig. 3(b)]. Thus we get across one and only one way—either horizontally with blacks on the lattice, or vertically with whites on the matching lattice—and hence Eq. (4.3a) follows.

Equation (4.3b) is similar. Now if black sites span in *both* directions, white paths on the matching lattice cannot span in *either* direction; if black sites do not span in both directions, white sites will span in one or the other direction on the matching lattice.

This matching property implies that the fixed point of R_2, and the fixed point of R_0 on the matching lattice, are complements (i.e., they add up to 1). This follows on evaluating Eq. (4.3b) at p^*, the fixed point of R_2,

$$R_0^M(1-p^*) = 1 - R_2(p^*) = 1 - p^* \ , \tag{4.4}$$

which shows that $(1-p^*)$ is the fixed point of R_0 on the matching lattice. Also, the eigenvalues of the two transformations, on their respective lattices, are equal. This follows again from Eq. (4.3b), first taking a derivative with respect to p, and using $-d/dq = d/dp$ to obtain

$$\left.\frac{dR_2(p)}{dp}\right|_{p=p^*} = \left.\frac{dR_0^M(q)}{dq}\right|_{q=1-p^*} . \tag{4.5}$$

Thus the scaling power $y_p = \nu_p^{-1}$ is the same on both lattices.

By the same reasoning, the fixed point obtained with R_1 on a particular lattice is complementary to the fixed point R_1 gives on the matching lattice; again y_p is the same for the two lattices. The above results are consistent with the matching property[44] that $p_c + p_c^M = 1$ (where p_c^M is the critical concentration on the matching lattice) and is also consistent with universality, in that y_p is independent of lattice type in a given dimension d. We also note that on any self-matching lattice (like the triangular lattice) the use of R_1 must always give $p^* = \frac{1}{2}$, since $R_1\ (p = \frac{1}{2}) + R_1\ (q = 1 - p = \frac{1}{2}) = 1$, implies $R_1\ (\frac{1}{2}) = \frac{1}{2}$. This explains Yuge's result[22] of $p^* = \frac{1}{2}$ on the triangular lattice.

We turn now to the transformation of Eq. (4.1b) for the ghost field. To define R_h, we consider the connectivity from a cell *to the ghost site*. We must be able to get into the cell (probability p' on the cell level) *and* to the ghost (probability h' that the renormalized ghost bond is occupied). On the site level, however, there are several ways one can get into the cell, and thus we have defined three rules for lattices with square cells. We must reach the ghost by approaching the cell: H_1: from a *single* direction (e.g., horizontally); H_2: *either* horizontally or vertically; or H_4: from *any* of the four edges. We will consider primarily H_2 in this paper.

TABLE I. Renormalization-group transformation $p' = R_p(b:p,h=0)$, evaluated in closed form on the square lattice, using rule R_0, for $b = 2$, 3, 4, and 5. Note $q \equiv 1 - p$.

b	$R_p(b:p,h=0)$
2	$p^4 + 4p^3q + 4p^2q^2$
3	$p^9 + 9p^8q + 36p^7q^2 + 82p^6q^3 + 93p^5q^4 + 44p^4q^5 + 6p^3q^6$
4	$p^{16} + 16p^{15}q + 120p^{14}q^2 + 560p^{13}q^3 + 1818p^{12}q^4 + 4296p^{11}q^5 + 7196p^{10}q^6 + 8136p^9q^7 + 5988p^8q^8 + 2784p^7q^9 + 780p^6q^{10} + 120p^5q^{11} + 8p^4q^{12}$
5	$p^{25} + 25p^{24}q + 300p^{23}q^2 + 2\,300p^{22}q^3 + 12\,650p^{21}q^4 + 53\,128p^{20}q^5 + 176\,992p^{19}q^6 + 478\,316p^{18}q^7 + 1\,054\,923p^{17}q^8 + 1\,880\,864p^{16}q^9 + 2\,666\,712p^{15}q^{10} + 2\,963\,364p^{14}q^{11} + 2\,556\,058p^{13}q^{12} + 1\,699\,665p^{12}q^{13} + 865\,132p^{11}q^{14} + 333\,630p^{10}q^{15} + 95\,845p^9q^{16} + 19\,916p^8q^{17} + 2\,836p^7q^{18} + 248p^6q^{19} + 10p^5q^{20}$

TABLE II. Renormalization-group transformation $p' = R_p(b:p,h=0)$, evaluated in closed form on the square lattice, using rule R_1, for $b=2$, 3, and 4.

b	$R_p(b:p,h=0)$
2	$p^4+4p^3q+2p^2q^2$
3	$p^9+9p^8q+36p^7q^2+67p^6q^3+59p^5q^4+22p^4q^5+3p^3q^6$
4	$p^{16}+16p^{15}q+120p^{14}q^2+560p^{13}q^3+1752p^{12}q^4+3736p^{11}q^5+5414p^{10}q^6+5272p^9q^7+3416p^8q^8+1452p^7q^9+390p^6q^{10}+60p^5q^{11}+4p^4q^{12}$

Which rule we choose from each set (R_0, R_1, or R_2; H_1, H_2, or H_4), for any given b, affects the form of our recursion relations (4.1a) and (4.1b) and hence p^*, λ_p, and λ_h. All, however, lead to reasonably good approximations. More significantly, the trend as $b \to \infty$ of all these rules is to the *same* ultimate value of p_c, and the scaling powers y_p and y_h. Thus, for large cell PSRG's, one is free to choose those connectivity rules for which calculations are most readily performed (generally R_1 and H_1).

B. Closed-form enumeration of the recursion relations

The closed-form, $h=0$, polynomial recursion relations for p' [cf. Eq. (4.1a)] according to R_0, R_1, and R_2 on the square lattice, are listed in Tables I–III, respectively. For R_1 and R_2 we have calculated the cases $b=2$, 3, and 4 while for R_0 we have also calculated $b=5$. By Eq. (4.3), these recursion relations (with the roles of p and q reversed) also apply to the square matching lattice.

The closed-form, general h, recursion relations for h' [cf. Eq. (4.1b)] according to H_1, H_2, and H_4 on the square lattice are listed in Tables IV–VI. We have calculated these recursion relations for $b=2$, 3, and 4.

To show how these recursion relations are obtained, we demonstrate the calculation for the 2×2 cell using R_0 and H_2. Unlike the recursion relations in Tables I–III, here we also include h in the p' calculation, in order to obtain the full, coupled set of equations. A 2×2 cell, with additional ghost bonds, is transformed into a renormalized site and a renormalized ghost bond as in Fig. 4.

The calculation of the renormalized site-occupation probability p' now reduces to the enumeration of the set of all possible configurations of sites and ghost bonds that span the cell. Using R_0, we obtain

$$p' = p^4+4p^3q+4p^2q^2+2p^2q^2h^2 \quad . \tag{4.6a}$$

In the first three terms on the right, we have enumerated all the ways of traversing the cell for which no h bonds are required. In these cases, the site configuration alone spans, and so explicit enumeration of *all* the possible ghost-bond states simply provides a factor of unity. Thus, we only consider h when it is explicitly needed to span. The p^4 term gives the probability that all four sites are occupied, and this configuration certainly spans the cell. The term $4p^3q$ corresponds to the four possible configurations which are missing exactly *one* site. Each of these configurations occurs with probability p^3q, and each spans the cell. For two sites missing, there are six possible configurations, four of which enable one to traverse the cell by R_0, regardless of the h

TABLE III. Renormalization-group transformation $p' = R_p(b:p,h=0)$, evaluated in closed form on the square lattice, using rule R_2, for $b=2$, 3, and 4.

b	$R_p(b:p,h=0)$
2	p^4+4p^3q
3	$p^9+9p^8q+36p^7q^2+52p^6q^3+25p^5q^4$
4	$p^{16}+16p^{15}q+120p^{14}q^2+560p^{13}q^3+1686p^{12}q^4+3176p^{11}q^5+3632p^{10}q^6+2408p^9q^7+844p^8q^8+120p^7q^9$

TABLE IV. Recursion relations for the ghost field using rule H_1, for cells of side $b=2$, 3, and 4. We use the notation $h_l \equiv [1-(1-h)^l]$ for the probability of reaching the ghost from a group of l sites. Note $h_1 = h$. This form is useful for determining λ_h, since the linear part of h_l is lh.

b	$p'h'$
2	$p^4h_4+4p^3qh_3+p^2q^2(2h+3h_2)+2pq^3h$
3	$p^9h_9+9p^8qh_8+p^7q^2(2h_6+34h_7)$ $+p^6q^3(3h+3h_2+3h_3+5h_4+13h_5+56h_6)$ $+p^5q^4(15h+14h_2+15h_3+25h_4+51h_5)$ $+p^4q^5(30h+25h_2+25h_3+31h_4)$ $+p^3q^6(30h+20h_2+14h_3)$ $+p^2q^7(15h+6h_2)+3pq^8h$
4	$p^{16}h_{16}+16p^{15}qh_{15}+p^{14}q^2(2h_{13}+118h_{14})$ $+p^{13}q^3(2h_{10}+4h_{11}+32h_{12}+522h_{13})$ $+p^{12}q^4(4h+6h_2+6h_3+7h_4+6h_5+8h_6+8h_7+13h_8+28h_9+54h_{10}+210h_{11}+1469h_{12})$ $+p^{11}q^5(44h+62h_2+62h_3+70h_4+70h_5+86h_6+108h_7+166h_8+288h_9+730h_{10}+2670h_{11})$ $+p^{10}q^6(220h+290h_2+288h_3+316h_4+338h_5+410h_6+532h_7+806h_8+1500h_9+3242h_{10})$ $+p^9q^7(660h+808h_2+786h_3+834h_4+904h_5+1066h_6+1368h_7+1986h_8+2808h_9)$ $+p^8q^8(1320h+1484h_2+1386h_3+1398h_4+1460h_5+1606h_6+1850h_7+1871h_8)$ $+p^7q^9(1848h+1876h_2+1636h_3+1518h_4+1432h_5+1328h_6+1010h_7)$ $+p^6q^{10}(1848h+1652h_2+1292h_3+1040h_4+790h_5+462h_6)$ $+p^5q^{11}(1320h+1000h_2+658h_3+410h_4+188h_5)$ $+p^4q^{12}(660h+398h_2+196h_3+71h_4)$ $+p^3q^{13}(220h+94h_2+26h_3)+p^2q^{14}(44h+10h_2)+4pq^{15}h$

TABLE V. Recursion relations for the ghost field using rule H_2, for cells of side $b=2$, 3, and 4. We define $h_l \equiv [1-(1-h)^l]$.

b	$p'h'$
2	$p^4h_4+4p^3qh_3+p^2q^2(h+5h_2)+3pq^3h$
3	$p^9h_9+9p^8qh_8+p^7q^2(h_6+35h_7)+p^6q^3(h_3+2h_4+8h_5+73h_6)$ $+p^5q^4(h+5h_2+10h_3+22h_4+88h_5)+p^4q^5(8h+20h_2+32h_3+65h_4)$ $+p^3q^6(18h+29h_2+33h_3)+p^2q^7(16h+14h_2)+5pq^8h$
4	$p^{16}h_{16}+16p^{15}qh_{15}+p^{14}q^2(h_{13}+119h_{14})+p^{13}q^3(h_{10}+2h_{11}+17h_{12}+540h_{13})$ $+p^{12}q^4(h_6+2h_7+5h_8+14h_9+28h_{10}+122h_{11}+1648h_{12})$ $+p^{11}q^5(h_3+4h_4+11h_5+24h_6+48h_7+90h_8+166h_9+500h_{10}+3524h_{11})$ $+p^{10}q^6(h+7h_2+26h_3+61h_4+117h_5+209h_6+344h_7+568h_8+1300h_9+5375h_{10})$ $+p^9q^7(15h+70h_2+181h_3+335h_4+549h_5+845h_6+1262h_7+2262h_8+5920h_9)$ $+p^8q^8(84h+298h_2+616h_3+974h_4+1404h_5+1921h_6+2758h_7+4806h_8)$ $+p^7q^9(252h+712h_2+1221h_3+1670h_4+2089h_5+2477h_6+2983h_7)$ $+p^6q^{10}(462h+1050h_2+1490h_3+1709h_4+1724h_5+1489h_6)$ $+p^5q^{11}(546h+982h_2+1109h_3+973h_4+632h_5)$ $+p^4q^{12}(420h+570h_2+464h_3+240h_4)$ $+p^3q^{13}(204h+188h_2+84h_3)$ $+p^2q^{14}(57h+27h_2)+7pq^{15}h$

TABLE VI. Recursion relations for the ghost field using rule H_4, for cells of side $b=2$, 3, and 4. We define $h_l \equiv [1-(1-h)^l]$.

b	$p'h'$
2	$p^4h_4+4p^3qh_3+6p^2q^2h_2+4pq^3h$
3	$p^9h_9+9p^8qh_8+36p^7q^2h_7+84p^6q^3h_6+p^5q^4(h_4+125h_5)+p^4q^5(4h_3+122h_4)$ $+p^3q^6(6h_2+78h_3)+p^2q^7(4h+32h_2)+8pq^8h$
4	$p^{16}h_{16}+16p^{15}qh_{15}+120p^{14}q^2h_{14}+560p^{13}q^3h_{13}+p^{12}q^4(4h_{11}+1816h_{12})$ $+p^{11}q^5(44h_{10}+4324h_{11})+p^{10}q^6(6h_8+216h_9+7786h_{10})$ $+p^9q^7(4h_6+48h_7+628h_8+10\,760h_9)$ $+p^8q^8(h_4+24h_5+168h_6+1208h_7+11\,469h_8)$ $+p^7q^9(4h_3+60h_4+336h_5+1624h_6+9416h_7)$ $+p^6q^{10}(6h_2+80h_3+420h_4+1568h_5+5934h_6)$ $+p^5q^{11}(4h+60h_2+336h_3+1096h_4+2872h_5)$ $+p^4q^{12}(24h+168h_2+548h_3+1079h_4)$ $+p^3q^{13}(48h+188h_2+320h_3)+p^2q^{14}(40h+74h_2)$ $+12pq^{15}h$

bonds. The two remaining configurations, in which only diagonally opposite sites are occupied, do not allow one to span the cell by nearest-neighbor bonds alone. However, we do get across these two configurations if we go from one site to the other via two ghost bonds,[36] and thus we obtain the $2p^2q^2h^2$ term of Eq. (4.6a).

The analogous calculation for rescaling the ghost-bond probability [cf. Eq. (4.1b)] is obtained by enumerating the configurations which enable us to reach the ghost. Using H_2 we obtain

$$p'h'=p^4[1-(1-h)^4]+4p^3q[1-(1-h)^3]$$
$$+5p^2q^2[1-(1-h)^2]+p^2q^2h+3pq^3h \quad . \quad (4.6b)$$

The left-hand side reflects that we must be able to enter the renormalized site, and travel up the renormalized ghost bond, to reach the ghost (cf. Fig. 4). On the right-hand side, the derivation of the p^2q^2 term will suffice as a demonstration of the method of calculation. There are six possible configurations with two sites occupied and two vacant. In five of these, we reach both the occupied sites by entering the cell from the two directions indicated in Fig. 4. The probability that neither ghost bond associated with these sites is occupied is $(1-h)^2$. Hence $[1-(1-h)^2]$ is the probability that we *do* reach the ghost, given one of these five-site configurations. Thus we obtain the $5p^2q^2[1-(1-h)^2]$ term in Eq. (4.6b) above. In the one remaining two-site configuration (sites 2 and 4 of Fig. 4 occupied) the probability that we reach the ghost is controlled by the single ghost bond emanating from site 2. Hence the term p^2q^2h of Eq. (4.6b) results.

This sort of manual enumeration procedure was used to calculate the R_0, R_1, and R_2 recursion relations for $b=2$ and 3, and the H_1, H_2, and H_4 recursion relations for $b=2$; for any larger cells, this procedure becomes prohibitively time consuming and error prone when done by hand. For this reason we have written computer programs which enumerate all possible configurations. By using a cluster multilabel-

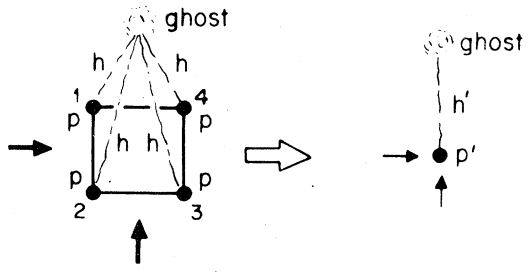

FIG. 4. Illustration of the rescaling of a 2×2 cell. The four original sites, each occupied with probability p, are transformed into a single renormalized site occupied with probability p'. If the original cell can be traversed in the directions indicated, the renormalized site is occupied according to rule R_0. The ghost bonds, which join to every site, are occupied with probability h. The probability of reaching the ghost, coming from the directions indicated, rescales the ghost bond according to H_2 (see text).

ing algorithm,[45] we determine if spanning by R_0, R_1, or R_2 occurs, and how many sites (and hence potential ghost bonds) are wetted by H_1, H_2, and H_4. However, even the computer can take us only a little further in these calculations. The 2^{b^2} configurations possible for a $b \times b$ cell, increases so rapidly with b, that only two additional cell sizes could be calculated in closed form. To illustrate the times involved, on a CDC 6600 computer calculation of the closed-form R_0 recursion relations takes approximately 0.5 sec for $b=3$, 60 sec for $b=4$, and 12 hours for $b=5$! For cells of size larger than 5 by 5 it is simply not feasible to calculate these recursion relations in closed form.

C. Monte Carlo calculation of the recursion relations

The physical interpretation of p' as the probability of spanning a cell whose sites are occupied with probability p, makes a numerical, Monte Carlo, evaluation of Eq. (4.1a) quite feasible for cells of considerably larger size than we could treat in closed form. We have obtained, in this way, an accurate numerical form of the transformation $p'=R_p(p)$ using R_0 and R_1, for b as large as 500 (cells of 250 000 sites). This procedure is a Monte Carlo renormalization group.[46]

The technique we have used is to take an array (cell) and fill it with random numbers in the interval (0,1). Our Monte Carlo program then asks the question, "At what p does this array *first* percolate?" (those sites whose random number is less than p being wetted, and the rest not). Repeating this procedure thousands of times, we obtain a distribution of p values which approximates the underlying probability density function, $L(b:p)$. We plot the numerical distribution which we obtain[47] with R_0 for a few values of b, in Fig. (5a). To obtain a feeling for how good such Monte Carlo calculations are, we show in Fig. 6 both the exact and the Monte Carlo results[47] for $L(b=5:p)$. (Using R_1, the analogous pictures are qualitatively the same, though with a somewhat smaller shift in the position of the peak as a function of b, primarily at small b.)

Our PSRG transformation defines p' as the *total* probability that we span at p, and thus is the *cumulative distribution function,* which is related to $L(b:p)$ by

$$p'=R_p(b:p,h=0)=\int_0^p L(b:\hat{p})\,d\hat{p}\ . \tag{4.7}$$

Thus the eigenvalue $\lambda_p=dR_p/dp\,|_{p=p^*}=L(b:p^*)$. However, because numerical approximation of $L(b:p)$ amounts to the creation of a discrete set of points, Eq. (4.7) becomes a sum.

In Fig. 5(b) we plot $R_p(b:p,h=0)$ obtained in this way using R_0, for the same values of b shown in Fig. 5(a). In Fig. 6, the Monte Carlo curve $R_p(b=5:p,h=0)$ is seen to be indistinguishable from the closed-form result.

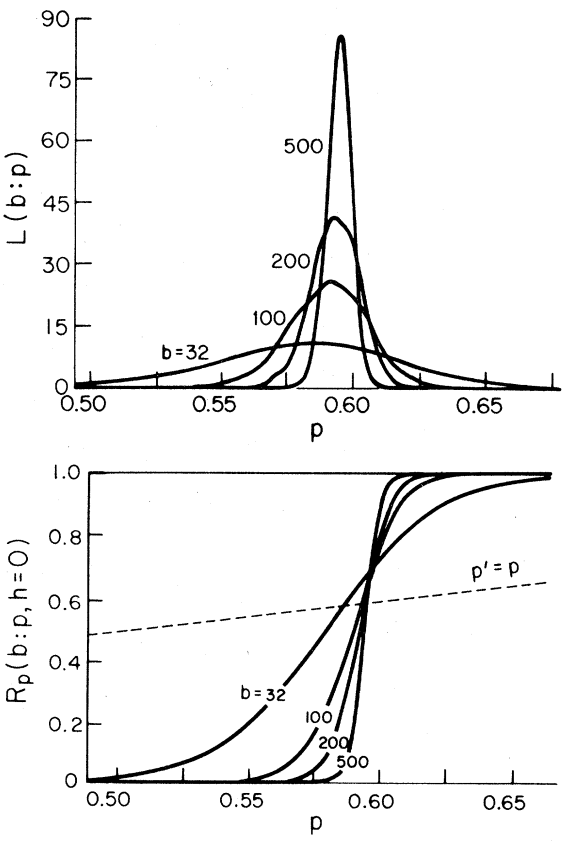

FIG. 5. (a) Probability density functions, $L(b:p)$, for $b=32$, 100, 200, and 500. $L(b:p)\,dp$ gives the probability of first spanning a $b \times b$ cell in the range from p to $p+dp$. These curves were calculated numerically by Monte Carlo methods, using R_0 (spanning in either direction). (b) The renormalized probability $p'=R(b:p,h=0)$ of spanning a $b \times b$ cell using R_0, for the same values of b as in (a). These curves are obtained numerically by integrating (summing the histograms) $L(b:p)$ of part (a). The intersection of these curves with the line $p'=p$ (dashed) gives the fixed point value p^* of these transformations. The slope of these curves at their respective values of p^* is just $L(b:p^*(b))$, and is the "thermal" eigenvalue λ_p of the PSRG from which we calculate $\nu_p=\ln b/\ln \lambda_p$.

Next, to use Monte Carlo methods to calculate Eq. (4.1b) numerically, we note that in general [cf. Eq. (4.6b)]

$$p'h'=\sum_{\text{config}} p_i[1-(1-h)^{n_i}]=\langle 1-(1-h)^{n_i}\rangle\ , \tag{4.8}$$

where p_i is the probability of a class of site configurations, and n_i is the corresponding number of sites reachable in this type of configuration. Thus, n_i is the number of ghost bonds that need to be blocked if we are *not* to get to the ghost site. Linearizing

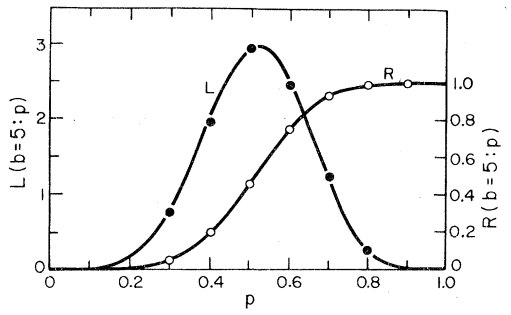

FIG. 6. Comparison of the Monte Carlo determined probability-density function $L(b=5{:}p)$, and cumulative distribution function $R_p(b=5{:}p,h=0)$, with the exact one for R_0. The Monte Carlo version is calculated by binning the spanning values of p into 100 bins of width 0.01 each, and averaging over adjacent bins. The resulting curve (here shown only as data points) is virtually indistinguishable from the exact curve (solid). $R_p(b=5{:}p,h=0)$ is simply the sum of $L(b=5{:}p)$ up to p. It is thus independent of binning, and as may be seen, is also indistinguishable from the closed-form (solid) curve.

Eq. (4.8),

$$h' = \langle n_i \rangle h/p' \ . \tag{4.9a}$$

Thus, a Monte Carlo calculation of

$$\lambda_h \equiv dh'/dh\Big|_{\substack{p=p^* \\ h=h^*=0}} = R_h(b{:}p^*,0) = \langle n_i \rangle / p^* \tag{4.9b}$$

involves only the calculation of the average over lattice configurations, of the number of sites wetted $\langle n_i \rangle$ by our particular rule. We do not need to randomly occupy ghost bonds as well, as these are treated exactly by Eq. (4.8).

V. LARGE-CELL PSRG RESULTS

We present the results of our PSRG for various cell sizes on the square lattice in Tables VII–IX. The results of rescaling the site-occupation probability according to the transformations R_0 and R_1 are presented in Tables VII and VIII, respectively. The transformation H_2 for the field leads to the eigenvalues λ_h and the scaling powers y_h given in Table IX.

We stop here for a moment to discuss operationally how we obtain λ_p and λ_h from the Monte Carlo PSRG. Recall that [see, e.g., below Eq. (4.7)] $\lambda_p = L(b{:}p^*)$, where $L(b{:}p)$ is the probability density for spanning a $b \times b$ cell at concentration p. Numerically we estimate $L(b{:}p)$ by sampling random arrays for their spanning thresholds, and then binning together the number that span in a given interval. This procedure generally results in a somewhat jagged $L(b{:}p)$. However, after thousands of Monte Carlo realizations, the jaggedness becomes considerably less severe [cf. Fig. 5(a)]. If the curve is too narrow (not enough resolution) or too wide (too few realizations per bin), we rebin the data. To smooth

TABLE VII. Exact and Monte Carlo results from $p' = R_p(b{:}p,h=0)$ using R_0 on the square lattice. The quantities $\langle p \rangle$ and σ refer to the mean and standard deviation of the underlying distribution $L(b{:}p)$. The fixed points of the PSRG transformations are labeled p^*. The eigenvalues $\lambda_p^{\rm vis}$—and derived from them the exponents $\nu_p^{\rm vis}$—are determined from $L(b{:}p^*)$. The vis refers to the Monte Carlo method of estimating $L(b{:}p^*)$ by binning and averaging data, and then visually fitting a smooth curve through the data points. We obtain λ_p^{β} as a closed-form approximation to λ_p from a β distribution having the same $\langle p \rangle$ and σ as $L(b{:}p)$. From the small cells we see that λ_p^{β} and ν_p^{β} are useful approximations. For large cells, they serve as unbiased estimates of $\lambda_p(b)$ and $\nu_p(b)$. Each Monte Carlo realization is a calculation of the value of p at which a $b \times b$ array of random numbers first percolates.

b	No. realizations	$\langle p \rangle$	σ	p^*	$\lambda_p^{\rm vis}$	λ_p^{β}	$\nu_p^{\rm vis}$	ν_p^{β}
2	Exact	0.4667	0.221 11	0.3820	1.528	1.522	1.635	1.650
3	Exact	0.4865	0.175 21	0.4726	2.069	2.059	1.511	1.521
4	Exact	0.5041	0.147 55	0.5093	2.543	2.523	1.485	1.498
4	99 980	0.5036 ± 0.0010	0.147 67 ± 0.000 30	0.5076 ± 0.0020	2.542 ± 0.025	2.520	1.486 ± 0.016	1.500
5	Exact	0.5170	0.128 39	0.5290	2.979	2.950	1.474	1.488
5	106 040	0.5168 ± 0.0007	0.128 16 ± 0.000 25	0.5282 ± 0.0008	2.980 ± 0.020	2.956	1.474 ± 0.009	1.485
8	92 975	0.5395 ± 0.0005	0.094 47 ± 0.000 20	0.5552 ± 0.0015	4.183 ± 0.035	4.108	1.453 ± 0.009	1.472
16	58 250	0.5623 ± 0.0002	0.058 50 ± 0.000 15	0.5749 ± 0.0010	6.775 ± 0.057	6.772	1.449 ± 0.007	1.449
32	15 585	0.5742 ± 0.0002	0.035 68 ± 0.000 21	0.5826 ± 0.0004	11.06 ± 0.10	11.16	1.442 ± 0.005	1.437
64	6 210	0.5824 ± 0.0002	0.021 33 ± 0.000 19	0.5875 ± 0.0003	18.72 ± 0.16	18.69	1.420 ± 0.004	1.420
100	3 855	0.5856 ± 0.0003	0.014 86 ± 0.000 18	0.5894 ± 0.0004	26.87 ± 0.35	26.83	1.399 ± 0.006	1.400
150	3 195	0.5875 ± 0.0003	0.011 36 ± 0.000 15	0.5905 ± 0.0004	36.40 ± 0.65	35.11	1.394 ± 0.007	1.408
200	1 830	0.5884 ± 0.0004	0.009 24 ± 0.000 16	0.5907 ± 0.0008	42.19 ± 1.0	43.17	1.416 ± 0.009	1.407
500	2 010	0.5905 ± 0.0002	0.004 621 ± 0.000 076	0.5918 ± 0.0005	87.35 ± 1.0	86.33	1.390 ± 0.004	1.394
∞ (extrap)	···	0.5931 ± 0.0006	···	0.5932 ± 0.0007	···	···	1.354 ± 0.012	1.357 ± 0.010

TABLE VIII. Exact and Monte Carlo results from $p' = R_p(b:p,h=0)$ using R_1. For a description of the quantities listed see Table VII.

b	No. realizations	$\langle p \rangle$	σ	p^*	$\lambda_p^{\rm vis}$	λ_p^{β}	ν_p^{vis}	ν_p^{β}
2	Exact	0.5333	0.221 11	0.618 04	1.528	1.522	1.635	1.650
3	Exact	0.5524	0.181 38	0.619 26	1.967	1.970	1.624	1.621
4	Exact	0.5640	0.154 83	0.619 35	2.370	2.381	1.607	1.598
4	80 000	0.5635 ± 0.0010	0.154 57 ± 0.000 34	0.618 1 ± 0.001 5	2.395 ± 0.035	2.386	1.587 ± 0.027	1.594
5	80 000	0.5713 ± 0.0010	0.135 42 ± 0.000 31	0.618 6 ± 0.001 5	2.777 ± 0.035	2.775	1.576 ± 0.019	1.577
32	7 995	0.5914 ± 0.0006	0.039 46 ± 0.000 33	0.601 9 ± 0.001 2	10.19 ± 0.19	10.08	1.493 ± 0.012	1.500
64	6 495	0.5926 ± 0.0004	0.023 11 ± 0.000 21	0.598 8 ± 0.000 4	16.83 ± 0.25	17.24	1.473 ± 0.008	1.461
100	2 880	0.5923 ± 0.0004	0.016 76 ± 0.000 23	0.596 8 ± 0.000 5	22.95 ± 0.50	23.79	1.470 ± 0.010	1.453
150	1 725	0.5927 ± 0.0005	0.012 27 ± 0.000 22	0.595 7 ± 0.000 5	32.51 ± 0.65	32.50	1.439 ± 0.009	1.439
200	1 005	0.5920 ± 0.0008	0.009 57 ± 0.000 22	0.594 7 ± 0.001 0	41.13 ± 3.0	41.68	1.426 ± 0.028	1.420
500	1 005	0.5926 ± 0.0005	0.005 10 ± 0.000 12	0.593 9 ± 0.001 0	78.9 ± 1.5	78.2	1.423 ± 0.006	1.426
∞	· · ·	0.5931 ± 0.0006	· · ·	0.593 0 ± 0.0007	· · ·	· · ·	1.340 ± 0.025	1.352
(extrap)								± 0.015

the curve further, we average over neighboring bins. Finally, we draw a smooth curve through the distribution, and thereby obtain an estimate for $L(b:p^*)$. These estimates are marked $\lambda_p^{\rm vis}$ in Tables VII and VIII.

The error bars on $\lambda_p^{\rm vis}$—and in fact on all our Monte Carlo data are derived by comparing the values obtained using different subsets of the data and taking the standard deviation. For the visual estimate of λ_p in particular, we have also compared the results obtained with different binnings of the same data. For each subset or rebinning of the data, the visually placed smooth curves through the distribution provide an additional measure of the error bar, since the less jagged the distribution the less uncertainty we have in placing the smooth curve.

There is, however, a certain degree of subjectivity in finding the best smooth curve to fit $L(b:p)$. For this reason we seek a closed-form distribution which could be used to approximate $L(b:p)$, from which we could then obtain objective estimates of λ_p. Such a closed-form distribution should ideally have parameters which could be fit to those properties of $L(b:p)$ that we can calculate most accurately. In particular, we are able to calculate very accurately the mean $\langle p \rangle$ and the variance $\sigma^2 \equiv (\langle p^2 \rangle - \langle p \rangle^2)$ of $L(b:p)$. Our first inclination, to use a Gaussian to fit $L(b:p)$, in fact works reasonably well for very large b. That it works less and less well for smaller b is not surprising, as a Gaussian is unbounded in its domain, whereas $L(b:p)$ is only defined for $p \in [0,1]$. It is pointless to have an unbiased estimate for λ_p based on such a model distribution, if it is clearly worse than the value of λ_p obtainable visually from the Monte Carlo for the true distribution. Furthermore, it is difficult to know when b is sufficiently large that we may trust the value of λ_p obtainable from the Gaussian.

We have instead turned to the β distribution,[48] defined by

$$B_{nm}(x) \equiv \frac{\Gamma(n+m)}{\Gamma(n)\Gamma(m)} x^{m-1}(1-x)^{n-1}, \quad 0 \leq x \leq 1 \ . \tag{5.1}$$

The mean and variance of this distribution are related to the parameters n and m by

$$\langle x \rangle = m/(m+n) \tag{5.2a}$$

and

$$\sigma^2 = mn/[(m+n)^2(m+n+1)] \ , \tag{5.2b}$$

and through the inverse formulas

$$n = [\langle x \rangle (1-\langle x \rangle) - \sigma^2](1-\langle x \rangle)/\sigma^2 \tag{5.3a}$$

and

$$m = n\langle x \rangle/(1-\langle x \rangle) \ . \tag{5.3b}$$

For large b the β distribution $B_{nm}(p)$ agrees exceedingly well with both the Monte Carlo data and the Gaussian approximation. However, even for small b—where we have exact expressions for $L(b:p)$—$B_{nm}(p)$ mimics the overall shape of the actual function almost perfectly.

One characteristic of the fit is worth noting, however. Whereas $p_{\max}$, the value of p at which the distribution is a maximum, and the mean, $\langle p \rangle$, are distinct for $L(b:p)$, the maximum of $B_{nm}(p)$ is forced to occur at $\langle p \rangle$. Because we adjust n and m so that the means of the two distributions coincide, we effec-

tively shift the maximum of $B_{nm}(p)$ over from the maximum of $L(b:p)$ by $(\langle p\rangle - p_{\max})$. Furthermore, because p^* lies quite close to $p_{\max}$, where $L(b:p)$ is essentially stationary, we make little error in assuming

$$\lambda_p = L(b:p^*) \simeq L(b:p_{\max}) \simeq [B_{nm}(p)]_{\max} = B_{nm}(\langle p\rangle) \quad . \tag{5.4}$$

TABLE IX. Results from rescaling the ghost field using H_2. Where error bars are not shown, the errors are smaller than the last significant digit shown.

b	p	No realizations	λ_h	y_h	η_p
2	0.592	Exact	3.834	1.9387	0.1226
2	0.593	Exact	3.834	1.9390	0.1220
2	0.594	Exact	3.835	1.9393	0.1214
3	0.592	Exact	8.317	1.9282	0.1436
3	0.593	Exact	8.322	1.9287	0.1426
3	0.594	Exact	8.326	1.9291	0.1418
4	0.592	Exact	14.37	1.9225	0.1550
4	0.593	Exact	14.38	1.9231	0.1538
4	0.594	Exact	14.39	1.9236	0.1528
5	0.592	80 000	21.92	1.918	0.1632
5	0.593	80 000	21.94	1.919	0.1620
5	0.594	80 000	21.97	1.920	0.1608
8	0.592	80 000	53.45	1.913	0.1732
8	0.593	80 000	53.55	1.914	0.1715
8	0.594	80 000	53.64	1.915	0.1699
16	0.592	80 000	198.3	1.908	0.1843
16	0.593	86 000	199.0	1.909	0.1816
16	0.594	80 000	199.7	1.910	0.1791
32	0.592	30 000	733.6 ± 0.2	1.904	0.1925 ± 0.0002
32	0.593	9 000	738.8 ± 0.2	1.906	0.1884 ± 0.0002
32	0.594	39 000	743.7 ± 0.1	1.908	0.1846 ± 0.0001
64	0.592	11 190	2722.5 ± 2.0	1.902	0.1964 ± 0.0003
64	0.593	21 390	2753.1 ± 5.0	1.904	0.1911 ± 0.0009
64	0.594	20 190	2785.2 ± 4.0	1.907	0.1855 ± 0.0007
100	0.592	9 008	6310 ± 5	1.900	0.2000 ± 0.0003
100	0.593	10 388	6426 ± 15	1.904	0.1920 ± 0.0009
100	0.594	9 008	6533 ± 10	1.908	0.1849 ± 0.0007
150	0.592	4 008	13497 ± 20	1.898	0.2040 ± 0.0006
150	0.593	5 418	13908 ± 70	1.904 ± 0.001	0.1920 ± 0.0020
150	0.594	2 508	14224 ± 75	1.908 ± 0.001	0.1831 ± 0.0021
200	0.592	1 008	23233 ± 20	1.8975	0.2051 ± 0.0003
200	0.593	2 088	24039 ± 80	1.904 ± 0.001	0.1922 ± 0.0013
200	0.594	1 008	24821 ± 75	1.9099 ± 0.001	0.1801 ± 0.0012
500	0.592	660	128 960 ± 50	1.893	0.2130 ± 0.0001
500	0.593	675	137 256 ± 750	1.904 ± 0.001	0.1930 ± 0.0018
500	0.594	672	144 980 ± 500	1.912 ± 0.001	0.1754 ± 0.0012
∞	0.592	...	...	−∞	∞
(extrap)	0.593	...	...	1.898 ± 0.003	0.204 ± 0.006
	0.594	...	...	2	0

In fact, since frequently p^* and $\langle p \rangle$ lie on opposite sides of $p_{\max}$, we would be badly underestimating λ_p by evaluating the β distribution at p^*. Estimates of λ_p made according to Eq. (5.4) are listed in Tables VII and VIII, under the column headed λ_p^β. Comparison of λ_p^β with λ_p^{vis} provides another estimate for the Monte Carlo errors.

This difficulty of obtaining an unbiased estimate is not present in calculating λ_h, which is obtained directly in the Monte Carlo program [cf. Eq. (4.9)]. The only ambiguity here is at what value of p to evaluate $\lambda_h = R_h(b:p,h=0)$. The obvious choice of p^* leaves open the question of which transformation—R_0, R_1, or R_2—to use in determining p^*. Since p^* is really only an approximation to p_c, we use $\lambda_h = R_h(b:p=p_c,h=0)$.

Having thus obtained λ_p and λ_h for various values of b (cf. Tables VII–IX), we recall our earlier discussion that larger cells should provide a better approximate PSRG transformation. This is indeed borne out upon comparison with series results. We note that our 5×5 cell (with its 2^{25} states) is larger than any cell used for closed-form PSRG calculations on the $d=2$ Ising model. Nevertheless, the values of p_c and ν_p we obtain still differ from series estimates by about 10% at this cell size. This is essentially the accuracy one has come to expect from PSRG techniques on these small cells. Of course, we have proceeded further and treated cells up to 500×500. Here accuracy (as compared with series) is on the order of 0.2% for p_c, and within a few percent for the exponents. However, even $b=500$ amounts to a one-shot approximation. We know that the error we have introduced at the surface is "small" because the cell is "large"; however, we have no quantitative way to estimate how small is "small". Fortunately, we are not limited to this one-shot approach.

A. Extrapolation of large-cell Monte Carlo PSRG results

Since we have PSRG results for a sequence of values of b, we may extrapolate our results to the $b\to\infty$ limit.[49] Although the PSRG itself becomes singular at $b=\infty$, our PSRG calculations are always for finite values of b. It is the result of successive *finite* transformations which we then extrapolate to obtain reliable estimates of the true values of p_c, y_p, and y_h.

We extrapolate the p^* sequence on a basis different from that on which we extrapolate y_p and y_h. In both cases, however, we discover power-law behavior. Thus it is not surprising that our analysis looks quite similar to the analysis of experimental data in the vicinity of a critical point.

Let us consider first $p^*(b)$. We expect from finite-size scaling considerations[50] that

$$[p_c^{\text{true}} - p^*(b)] \equiv \Delta p^* \sim b^{-1/\nu_p} \quad . \tag{5.5}$$

In Fig. 7 we plot p^* vs b^{-1/ν_t}, with a trial value of $\nu_t = 1.355$. This leads to an extrapolation for p_c^{true} at the intercept $b^{-1/\nu_t}=0$. As Fig. 7 shows, although R_0 and R_1 give different values for p^* at all finite values of b, the extrapolations of these to $b\to\infty$ essentially agree, giving $p_c = 0.5931 \pm 0.007$—consistent with but more accurate than the value $p_c = 0.593 \pm 0.002$ predicted by series.[51] We have also used other trial values for ν_p in Eq. (5.5). However, this is neither a sensitive way to determine the exponent ν_p, nor does the predicted value of p_c change appreciably for a range of reasonable choices of ν_p. Nevertheless, if we have found p_c^{true} accurately, we may return to Eq. (5.5) to see if our choice of ν_t was a reasonable one. In Fig. 8 we plot $\ln \Delta p^*$ vs $\ln b$, for R_0. Note that in the asymptotic region of Eq. (5.5), the uncertainty in Δp^* becomes comparable to Δp^* itself. Thus we use Fig. 8 only to give us confidence that the exponent in Eq. (5.5) is in fact ν_p.

For the extrapolation of the scaling powers y_p and y_h, we consider the eigenvalues λ_x calculated from the PSRG. Recall that the scaling powers were defined in terms of the eigenvalues through the relation

$$\lambda_x = b^{y_x} \quad , \tag{5.6}$$

where x is either p or h. We may write

$$\lambda_x^{\text{true}}(b) = A(b)\lambda_x^{\text{calc}}(b) \quad , \tag{5.7}$$

thereby defining $A(b)$, a "correction" whose magnitude (different from unity) is a measure of the accu-

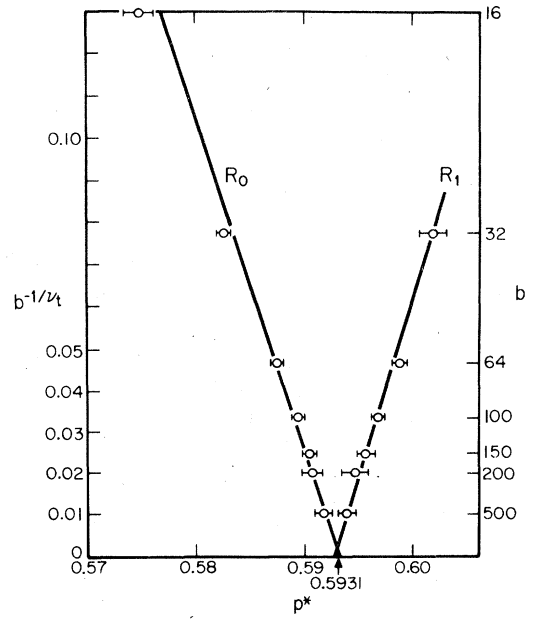

FIG. 7. Extrapolation of the sequence of fixed point $p^*(b)$ obtained from both rules R_0 and R_1. We have chosen the trial value of $\nu_t = 1.355$ for this plot.

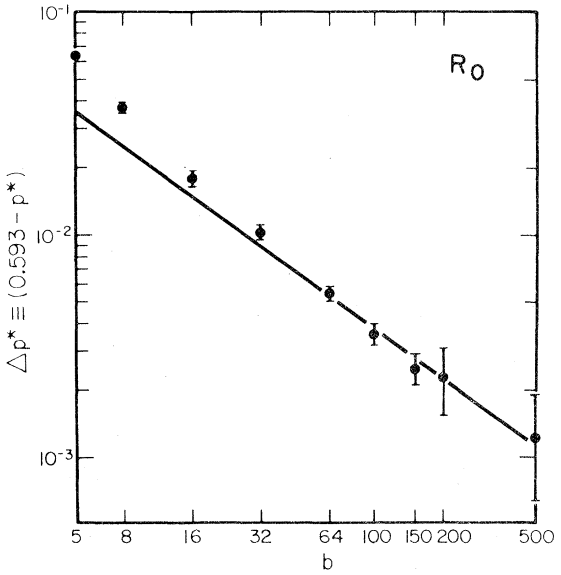

FIG. 8. Log-log plot of $\Delta p^* \equiv (0.5930 - p^*)$ against b, for rule R_0. There is initial curvature in this plot since $(p - p^*) \sim b^{-1/\nu_p}$ only asymptotically. For large b, the error in Δp^* is comparable to Δp^* itself. Thus we seek only to confirm that the exponent *is* ν_p. We find the inverse slope of this plot to be 1.3 ± 0.1.

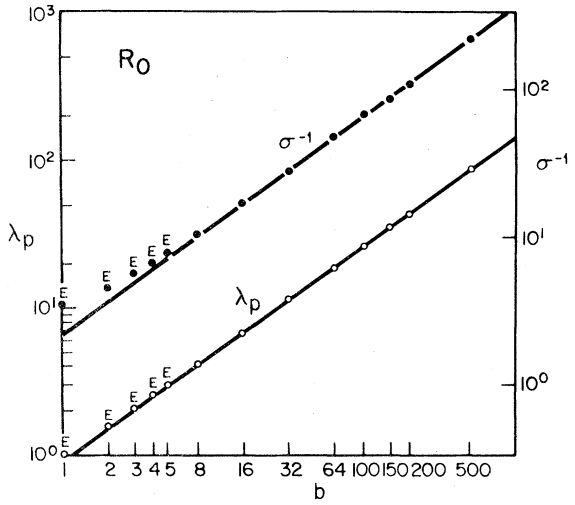

FIG. 9. Eigenvalue $\lambda_p(b)$ in a log-log plot against b. Points marked E are evaluated in closed form, while the remaining points are obtained from the β distribution. The slope gives $y_p = \nu_p^{-1}$. Also shown is the inverse width σ^{-1} of $L(b:p)$, which *asymptotically* should have the same slope. These plots were obtained using rule R_0.

racy of the approximation. Then [cf. Eq. (5.6)] $y_p^{\text{true}} = \ln A(b)/\ln b + y_p^{\text{calc}}$. Thus, if y_p^{calc} is to approach y_p^{true} as $b \to \infty$, we need only impose the relatively weak condition that $A(b)$ must either not tend to zero or infinity, or do so no faster than logarithmically. If $\ln A$ does not diverge, we assume $\ln A \to c$ or oscillates about c. Thus asymptotically,

$$y_x^{\text{calc}} = y_x^{\text{true}} - c/\ln b \tag{5.8a}$$

or

$$\ln \lambda_x^{\text{calc}}(b) = y_x^{\text{true}} \ln b - c \quad . \tag{5.8b}$$

Equation (5.8a) suggests that the sequence $y_x(b)$ should be extrapolated against the variable $1/\ln b$, and that in the asymptotic region where Eq. (5.8a) is valid, this should be a straight line with intercept y_x^{true}. Equation (5.8b) suggests that a plot of $\ln \lambda_x^{\text{calc}}(b)$ vs $\ln b$ should also be a straight line asymptotically, and this line should have a slope of y_x^{true}. These two equations are the basis of our extrapolation for determining the critical exponents.

In Fig. 9 we plot $\ln \lambda_p(b)$ vs $\ln b$. For $b \leq 5$ the values shown are the exactly calculated eigenvalues of the R_0 transformation, while $b \geq 8$ we have fit our Monte Carlo data for R_0 to a β distribution in order to obtain $\lambda_p(b)$ (see Table VII). From the inverse slope of this line we obtain $\nu_p = 1.357 \pm 0.010$. The same plot using the visually estimated values of λ_p, gives $\nu_p = 1.354 \pm 0.012$. These values should be compared to the series values[39,40] referred to above. Our error bars are obtained by comparing the results of least-square fits with successive data points removed from the set, and also with the values of the individual data points varied within their own error bars.

When we use R_1 as our "rule", we do not expect (nor do we find) that $\lambda_p(b)$, and hence $\nu_p(b)$, have the same values as we obtained from R_0. For a single-shot RG procedure this would be worrisome. One might wonder which rule is "correct". However, by extrapolating, as done here, we find that we obtain virtually the same ultimate value for ν_p regardless of the rule. For R_1 the analogous plot to Fig. 9 gives $\nu_p = 1.352 \pm 0.015$, while using visually obtained estimates for $\lambda_p(b)$ we find $\nu_p = 1.340 \pm 0.025$.

In Fig. 10 we extrapolate y_p by following Eq. (5.8a). For both R_0 and R_1 we plot y_p vs $1/\ln b$, once again using the values of λ_p determined from the β distribution. Here too we find "rule independence" in the limit $b \to \infty$. Asymptotically R_0 heads toward $\nu_p = y_p^{-1} = 1.354 \pm 0.014$ while R_1 seems to point at $\nu_p = 1.356 \pm 0.025$. Here the error bars represent confidence limits much like those obtained when extrapolating the results from series expansions. We obtain these confidence limits by first noting that a number of straight lines may be made to fit the data points when their individual error bars are taken into account, and when the number of data points is varied by the choice of the "asymptotic regime". The lines which fit the data with the greatest and smallest intercepts are used to provide the confi-

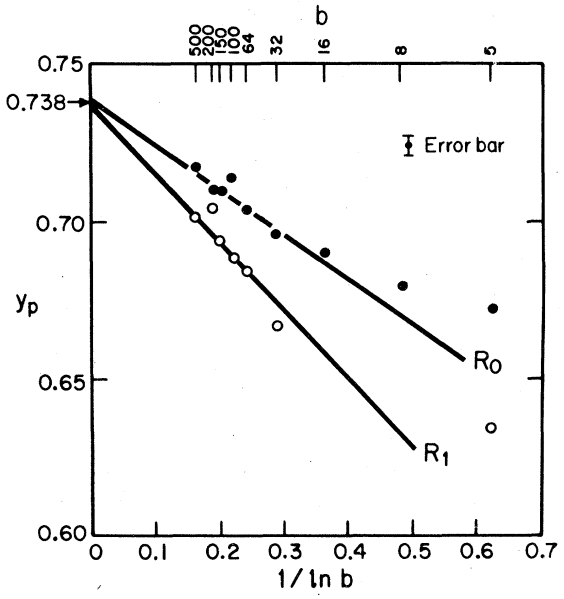

FIG. 10. Extrapolation against $1/\ln b$, for y_p determined from the β distribution. Results for both R_0 and R_1 are shown. Note that for finite b, both rules are off from y_p^{true}, but both approach approximately the same final value of $y_p = 0.738$, as $b \to \infty$. The representative error bar shown derives from the uncertainty in the β distribution due to error bars on $\langle p \rangle$ and σ.

dence limits.

In Fig. 11 we show, for the field eigenvalue, a plot of $\ln \lambda_h(b)$ vs $\ln b$. We have calculated $\lambda_h(b)$ according to the transformation H_2, with the eigenvalue evaluated at $p = 0.593$ (see Table IX). Note how exceptionally linear this plot is. From the slope of this line we estimate $y_h = 1.899 \pm 0.002$. In Fig. 12 we show the $1/\ln b$ extrapolation of y_h. From the intercept at $1/\ln b = 0$ we estimate

$$y_h = d(1+\delta^{-1})^{-1} = \beta\delta\nu^{-1} = 1.897(+0.003, -0.002)$$

As discussed earlier, there is an ambiguity as to the value of p at which to evaluate λ_h. We decided to use $p = p_c$. However, we do not know p_c exactly. To determine how sensitive y_h is to the correct choice of p_c we evaluated λ_h at $p = 0.592$, 0.593, and 0.594 (see Table IX). As expected, for small b, y_h is not very sensitive at all to the choice of p. However at large b, a small change in p causes a large change in how many sites are "wetted", and hence in λ_h. In fact this behavior, which can be clearly seen in Fig. 12, may be used as a sensitive way to determine p_c. From Fig. 12 we estimate $p_c = 0.5930 \pm 0.0005$.

We may understand the behavior in Fig. 12 if we recall that [cf. Eq. (4.9)]

$$\lambda_h = \langle n_i \rangle / p \simeq b^d p P(p,b)/p = b^d P(p,b) \quad .$$

Thus $y_h = d + \ln P(p,b)/\ln b$. At $p = p_c$, $P(p_c,b) \sim b^{-\beta_p/\nu_p}$ (see below), and so $y_h = d - \beta_p/\nu_p$. This is the correct asymptotic behavior. If, however, we are at $p > p_c$, $P(p,b) \to$ const, and $y_h = d + \ln(\text{const})/\ln b \to d$. Hence in Fig. 12 we see the curve marked 0.594 initially heading toward y_h^{true}, for the small cells do not yet "know" that $0.594 > p_c$. The large cells "know", and $y_h \to 2$. Likewise, when $p < p_c$, $P(p,b) \to 0$ faster than $b^{-\beta_p/\nu_p}$ (almost certainly faster than any power[52] of b). Thus we expect, in the limit $b \to \infty$, $y_h \to -\infty$. Again in Fig. 12, we see the curve marked 0.592 initially heading toward y_h^{true}, but now y_h drops lower and lower.

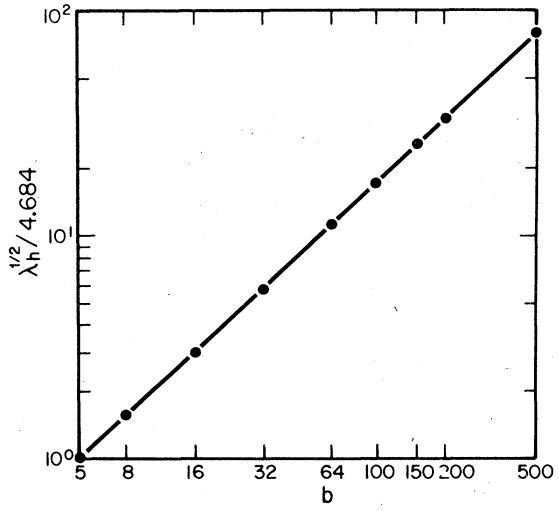

FIG. 11. Log-log plot of the magnetic eigenvalue $\lambda_h(b)$ against b. Note the extreme linearity of this plot. From the slope we determine the scaling power y_h.

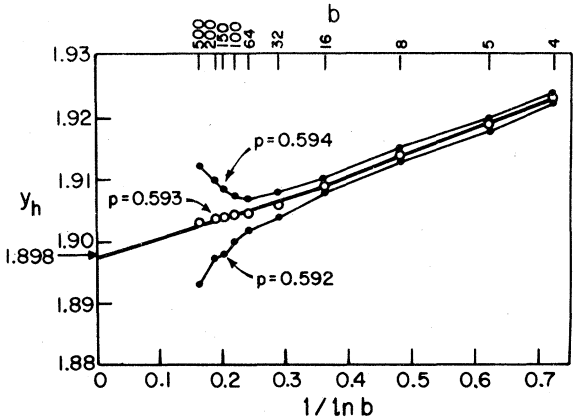

FIG. 12. Extrapolation against $1/\ln b$ of y_h determined by evaluating the H_2 recursion relations, for h' at $p = 0.592$, 0.593, and 0.594. Initially y_h is not sensitive to the correct choice of p_c. However, deviation from a straight line becomes quite apparent for $b \geq 32$. This plot for y_h is analogous to the plot shown in Fig. 10 for y_p.

B. Connection with finite-size scaling

Thus far we have presented the PSRG analysis. However, in the process of determining the recursion relations we generate ρ Monte Carlo realizations, where $b^2\rho \geq 10^7$. The renormalization function $R_p(b:p,h=0)$ was calculated by integrating $L(b:p)$. However $R_p(b:p,h=0)$ may be treated in a purely statistical sense[53] as may $L(b:p)$.[54] In this case $L(b:p)$ is the probability density function, while $R_p(b:p,h=0)$ is the cumulative distribution function. For each b, we have calculated the mean, $\langle p \rangle$, of $L(b:p)$ and the standard deviation from the mean, $\sigma \equiv \langle (p - \langle p \rangle)^2 \rangle^{1/2}$. It was these values that we used to fit the β distribution to $L(b:p)$.

However, the mean is itself an estimate for p_c. Further, for large b both $(\langle p \rangle - p_c^{\text{true}})$ and σ should scale[54] as b^{-1/ν_p}. Thus, in Fig. 13 we have plotted $\langle p \rangle$ vs b^{-1/ν_t}, with $\nu_t = 1.355$, in complete analogy with the plot for p^* in Fig. 7. Both R_0 and R_1 essentially agree, giving an extrapolated value of $p_c = 0.5931 \pm 0.0006$. To see that σ scales as it should, we have plotted, in Fig. 9, $\ln \sigma^{-1}$ vs $\ln b$ for the σ values obtained from the transformation R_0 (Table VII). (We have plotted it on the same graph as the eigenvalue λ_p for comparison.) From the inverse slope we find $\nu_p = 1.355 \pm 0.013$.

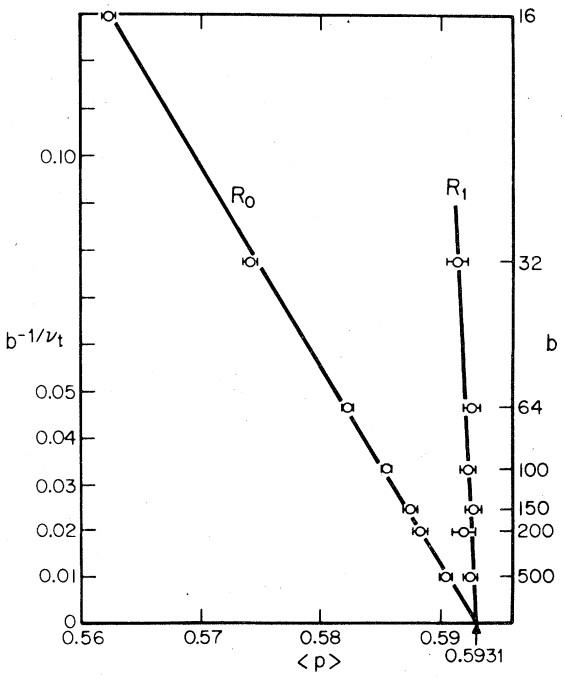

FIG. 13. Finite-size scaling extrapolation of the sequence of means $\langle p \rangle$ at which one first spans $b \times b$ cells, for both rules R_0 and R_1. We have chosen the trial value of $\nu_t = 1.355$. The plot is similar to Fig. 7 where $p^*(b)$ is extrapolated.

We see here a rather intimate relationship between finite-size scaling and the renormalization group.[55] The "thermal" eigenvalue of the PSRG is the value, $L(b:p^*)$, of the density function at $p = p^*$. As b increases, this approaches a constant times the value, $L(b:p_{\max})$, of the density function at its peak. The limiting value of $L(b:p^*)/L(b:p_{\max})$ appears to be very close to one. Because the integral over the entire density function is unity, $L(b:p_{\max}) \to 1/[(2\pi)^{1/2}\sigma]$ if the function approaches a Gaussian, as it seems to, and in general $\lambda_p \to \text{const}/\sigma$. Then, the renormalization-group statement that $\nu_p = \ln b / \ln \lambda_p$ implies finite-size scaling: asymptotically (for large b), $-\nu_p \ln \sigma = \ln b + \text{const}$. From a log-log plot, with at least two values of b, this constant may be eliminated, and ν_p determined. Our two values of b must, of course, both be in the asymptotic region, or we will not eliminate the constant properly. The renormalization group, on the other hand, chooses λ_p (its "σ-like" parameter) in such a way that if σ is replaced by λ_p^{-1} the constant is zero, and we need not be in any asymptotic region. This is because λ_p $(b=1) \equiv 1$, since the eigenvalue of the identity transformation is unity. One might say that the renormalization group "knows" *a priori* its eigenvalue at one other value of b, $b = 1$. However, since our λ_p^{calc} is only an approximation to λ_p^{true}, asymptotically the intercept need not be zero with the renormalization group either [cf. Eq. (5.8b)] though it is expected to be close in order that the small cell PSRG makes sense. Thus, only asymptotically need

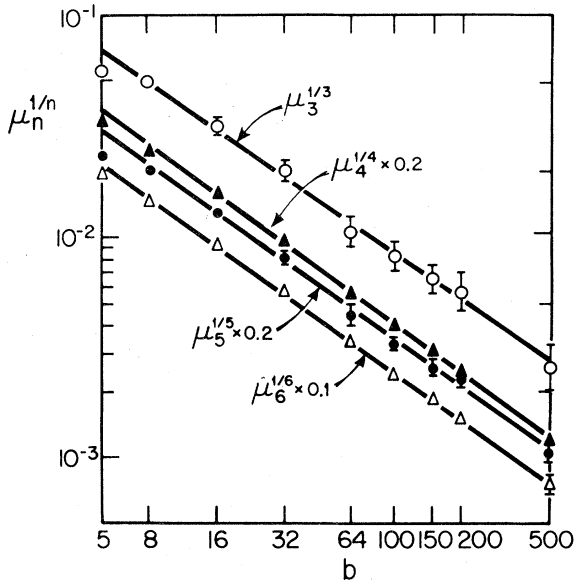

FIG. 14. Log-log plot of the nth roots of the nth central moments of $L(b:p)$ using R_0 for $n = 3$, 4, 5, and 6. The inverse slopes of all the plots shown are consistent with $\nu_p \simeq 1.35$.

the slope of $\ln \lambda_p$ vs $\ln b$ actually become ν_p^{-1}. However, we now expect the asymptotic region to be reached for considerably smaller b than for ordinary Monte Carlo.

We have also calculated the moments $\langle p^n \rangle$ and central moments $\mu_n \equiv \langle (p - \langle p \rangle)^n \rangle$ of $L(b:p)$, for $n = 1, 2, \ldots, 9$. From finite-size scaling we expect *all* "p-like" quantities to vanish as b^{-1/ν_p}. In Fig. 14 we show a log-log plot of $\mu_n^{1/n}$ against b for $n = 3$, 4, 5, and 6. For the case $n = 2$ we have already seen this plot in Fig. 9, as $\sigma = \mu_2^{1/2}$. The curves shown in Fig. 14 were obtained using R_0.

Furthermore, extrapolation of the field eigenvalue λ_h is also closely related to finite-size scaling. For sufficiently large b [see Eq. (4.9)] $\lambda_h \to b^d P(p_c,b)$. Thus the renormalization group tells us that for large b, $y_h = d + \ln P(p_c,b)/\ln b$. Since $y_h = d - \beta_p/\nu_p$ from ordinary scaling, we have derived the finite-size scaling result that $P(p_c,b) \sim b^{-\beta_p/\nu_p}$.

VI. DISCUSSION

We have shown that one may use large-cell (Monte Carlo) PSRG as an accurate numerical method. In particular, for the site percolation problem on the square lattice, we have discovered that even the simplest one-parameter approximation becomes progressively better as we increase b. We further noted that the trend is so smooth that one may readily extrapolate to the limit $b \to \infty$. As expected, the final results for the critical parameters are virtually the same for all the different connectivity weight functions used.

To obtain p_c, we calculate p^* from the PSRG. Then we extrapolate these fixed-point values as a function of b, in analogy with the usual extrapolation by finite-size scaling done for p_c of a finite system[50,53,54] (which is shifted from the true p_c). However, each p^* already corresponds to the fixed point of the infinite system, since renormalization proceeds through all length scales by interation. Thus it is perhaps surprising that finite-size scaling should apply here. However, finite-size effects do enter in the approximation, as noted in Sec. III. If we could in fact write down the exact recursion relation we would obtain $p^* = p_c$ exactly, for *all* b.

To obtain the critical exponents we calculate the scaling powers y_p and y_h. For large values of b these values, as well as the p^* values, are in good agreement with series (within a few percent or better). However, to obtain the best accuracy we extrapolate to $b \to \infty$. We do this extrapolation in two separate ways [cf. Eqs. (5.8a) and (5.8b)]. These methods, in the $b \to \infty$ limit, turn out to be intimately connected to finite-size scaling, though only the PSRG continues to have meaning even for small b.

Our best estimates for the two scaling powers are $y_p = 0.7385 \pm 0.0080$ and $y_h = 1.898 \pm 0.003$, from which we obtain

$$\alpha_p = -0.708 \pm 0.030, \quad \beta_p = 0.138(+0.006, -0.005) ,$$
$$\gamma_p = 2.432 \pm 0.035, \quad \delta_p = 18.6 \pm 0.6 ,$$
$$\nu_p = 1.354 \pm 0.015 , \tag{6.1}$$

and

$$2 - \eta_p = 1.796 \pm 0.006 ,$$

which compare well with estimates obtained by other methods.[39,40,56–58] The site percolation threshold is found for the square lattice at

$$p = 0.5931 \pm 0.0006 . \tag{6.2}$$

We note that our error bars, which are to be interpreted as confidence intervals, are roughly comparable to those obtained from series methods. In particular, our estimates of p_c, ν_p, and δ_p are more accurate than estimates afforded by series. Furthermore, because of the essential simplicity of the method, this technique is flexible and readily modified to treat other lattices[8,30,59] as well as other types of percolation problems.[60,61]

Currently there exists a controversy over the true value of ν_p. Various authors[31,32] have proposed "exact" values for ν_p. Klein *et al.*[32] argue that

$$\nu_p = \ln \sqrt{3}/\ln(\tfrac{3}{2}) = 1.3547 \cdots , \tag{6.3a}$$

while more recently den Nijs has put forth a conjecture which leads to[31]

$$\nu_p = \tfrac{4}{3} . \tag{6.3b}$$

Our numerical work clearly favors the former value for ν_p, but can by no means entirely eliminate the possibility of the latter.

Finally, in this regard we should note a related controversy. Domb and Pearce[62] have done a series calculation for α_p, using a novel type of transformation technique[63] from which they claim $\alpha_p = -0.668 \pm 0.004$—with 50 times tighter error bars than previous series calculations[12] of α_p. Hyperscaling then implies a value of $\nu_p = 1.334 \pm 0.002$, lending support to the den Nijs conjecture. However, the result of Domb and Pearce is completely inconsistent with other series work.[57,58] In particular, the most recent series calculations of[57] $\gamma_p = 2.425 \pm 0.005$ and[58] $\beta_p = 0.139 \pm 0.003$ lead to (using the Rushbrooke equality) $\alpha_p = -0.703 \pm 0.011$. This latter value is entirely consistent with our PSRG results [Eq. (6.1)] and implies a value of $\nu_p = 1.352 \pm 0.006$ which is consistent with Klein *et al.* as well as with our numerical results here, though not with den Nijs' conjecture.

ACKNOWLEDGMENTS

It is a pleasure to thank Antonio Coniglio, Hisao Nakanishi, Sidney Redner, and Gerald Shlifer for many useful discussions in the course of this work. We are also grateful to the Boston University Academic Computing Center and to the Air Force Geophysics Lab for the many hours of computer time which were made available to us. Finally, Dietrich Stauffer is to be thanked for a careful reading and detailed criticism of a draft of this paper. This work was supported in part by ARO and AFOSR.

APPENDIX A: CLOSED-FORM LARGE-CELL PSRG: ONE-DIMENSIONAL PERCOLATION WITH MULTINEIGHBOR BONDS

An ideal test of the large-cell PSRG approach would be an exactly soluble model whose PSRG recursion relations may be obtained in closed form for arbitrary rescaling length b. We would be able to determine if, in fact, the limit as $b \to \infty$ of the various critical parameters [e.g., $p_c(b)$, $\nu_p(b)$, $\alpha_p(b)$, $\beta_p(b) \cdots$] gives the exact results. At least one such model exists: site percolation on a linear-chain lattice with bonds between nearest neighbors, next-nearest neighbors, etc., up to Lth-nearest neighbors. The exact solution for p_c and ν_p is known.[33] Here we present the PSRG analysis for arbitrary b. However, before we treat this model by the PSRG it is helpful to review the special case[35] $L=1$—the ordinary linear chain.

For $L=1$ we renormalize a cell of b sites to a single site [see Fig. 15(a)]. The individual sites are occupied with probability p; the renormalized "cell spins" are occupied with probability p'. We perform the renormalization transformation by preserving connectivity. Hence a cell is occupied if we can traverse the cell by being able to "flow" from the external site marked 1 to the external site marked 2. We find p' by writing the traversal condition on both the cell and the site levels. We obtain $p'=p^b$, where the left-hand side is the probability that we can traverse the cell on the cell level, while the right-hand side is the probability that we can traverse the cell on the site level. The solution to this recursion relation is $p^*=1$ and $\nu_p=1$, independent of b. Hence we may take the limit $b \to \infty$ trivially, and the result $p_c=1$, $\nu_p=1$ agrees with the known exact result.[35] Note that in this ($L=1$) case p', the probability that a cell spin is occupied, may equally well be thought of as the probability of getting across the cell.

For $L>1$ we must be more careful. We can no longer meaningfully renormalize a cell of b sites to a single site [see Fig. 15(b)]. Although on the site level we can write an expression for the probability of traversing the cell from 1 to 2, on the cell level this is not possible because there is always a connected path from 1 to 2 by some further-neighbor bond—independent of the occupation of the cell spin! To make a meaningful renormalization group (RG) we need at least L cell spins in the renormalized block. Our cell must be at least as large as the range of the interaction [see Fig. 15(c)]. Now we find the RG recursion relations by equating the probability of traversing the cell on the site and cell levels. For example, for the case pictured [Fig. 15(c)] of $L=2$, we are rescaling from a three-site cell to a two-site cell. We have $b=\frac{3}{2}$ and

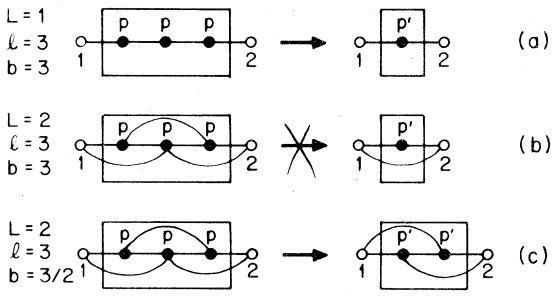

FIG. 15. (a) Three-site cell ($l=3$) on the nearest-neighbor ($L=1$) linear-chain lattice is renormalized to a single site. The rescaling factor is $b=3$. The recursion relation is determined by equating the probabilities on the site and cell levels of flowing through the cell from the point labeled 1 to the point labeled 2. (b) When next-nearest-neighbor bonds are present as well ($L=2$), the analogous transformation to a single site is not a valid one. This is because the probability of flowing from point 1 to point 2 in the renormalized picture is independent of the cell occupation probability p'. To have a meaningful transformation, our renormalized block must contain at least L (=2) renormalized sites. This is illustrated in (c), where now $b=\frac{3}{2}$.

$$p'^2+2p'q'=p^3+3p^2q+pq^2 \ , \tag{A1}$$

where $q \equiv 1-p$. The fixed point is at $p^*=1$. Differentiating, we obtain

$$\frac{q'}{q}\frac{dp'}{dp}=2p+\tfrac{1}{2}q \ . \tag{A2}$$

To find the eigenvalue $\lambda_p \equiv dp'/dp|_{p=p^*}$, we need to evaluate the left-hand side of Eq. (A2). First we must determine the ratio q'/q when q, $q' \to 0$. Note that

$$\begin{aligned}\lim_{q\to 0}\frac{q'(q)}{q} &= \lim_{p\to 1}\frac{1-p'(p)}{1-p} \\ &= \lim_{p\to 1}\frac{p'(p)-p'(1)}{p-1} \\ &= \left.\frac{dp'}{dp}\right|_{p=1} \ .\end{aligned} \tag{A3}$$

Thus $(dp'/dp)^2|_{p=1}=2$, $\lambda_p=\sqrt{2}$, and

$$\nu_p=\ln b/\ln \lambda_p=\ln(\tfrac{3}{2})/\ln\sqrt{2} \simeq 1.2 \ .$$

This is not the exact $L=2$ result of $\nu_p=2$. However, by going to larger cells we hope to improve this result.

Let us rescale from an arbitrarily large l-site cell to a two-site block. (Two sites is sufficiently large for the renormalized block since we are just treating $L=2$ now.) In analogy to Eq. (A1) we find

$$p'^2+2p'q'=p^l+lp^{l-1}q + [\tfrac{1}{2}l(l-1)-(l-1)]p^{l-2}q^2+O(q^3) \ , \tag{A4}$$

where the last term on the right comes from all possible pairs of two vacant sites, excluding the $(l-1)$ "two-in-a-row" pairs which break the connectivity. We first note that $p=p'=p^*=1$ is a fixed point. Differentiating Eq. (A4) we obtain

$$2q'\frac{dp'}{dp}=2(l-1)p^{l-2}q+O(q^2) \ . \tag{A5}$$

Thus [cf. Eqs. (A3) and (A5)]

$$\lim_{p\to 1}\frac{q'}{q}\frac{dp'}{dp}=\left(\left.\frac{dp'}{dp}\right|_{p=1}\right)^2=l-1 \ . \tag{A6}$$

We find the eigenvalue at $p^*=1$ to be,

$$\lambda_p=\left.\frac{dp'}{dp}\right|_{p=1}=\sqrt{l-1}>1 \ . \tag{A7}$$

The final inequality tells us that $p^*=1$ is in fact the relevant fixed point. Calculating $\nu_p(l)$, we obtain

$$\nu_p(l)=\frac{\ln b}{\ln\lambda_p}=\frac{\ln\frac{1}{2}l}{\ln(l-1)^{1/2}}=2\frac{\ln\frac{1}{2}l}{\ln(l-1)} \ . \tag{A8}$$

Thus our ν_p $(L=2)$ does in fact depend on the size l of the cell we start with. However,

$$\lim_{l\to\infty}\nu_p(l)=\lim_{l\to\infty}2\frac{\ln\frac{1}{2}l}{\ln(l-1)}=2, \quad L=2 \ , \tag{A9}$$

which is the exact result.[33]

We now derive the general case where all bonds up to Lth-nearest neighbors are present. We must renormalize to a cell which contains at least L renormalized sites, to have a meaningful cell-level picture. The probability of traversing this renormalized cell is just $(1-q'^L)$ since all L sites must be missing to prevent us from traversing. Thus, the transformation from an l-site cell to an L-site cell is

$$\begin{aligned}(1-q'^L)=p^l+lp^{l-1}q+[\tfrac{1}{2}l(l-1)]p^{l-2}q^2+\cdots \\ +\frac{l!}{(l-L+1)!(L-1)!}p^{l-L+1}q^{L-1} \\ +\left(\frac{l!}{(l-L)!L!}-(l-L+1)\right)p^{l-L}q^L \\ +O(q^{L+1}) \ ,\end{aligned} \tag{A10}$$

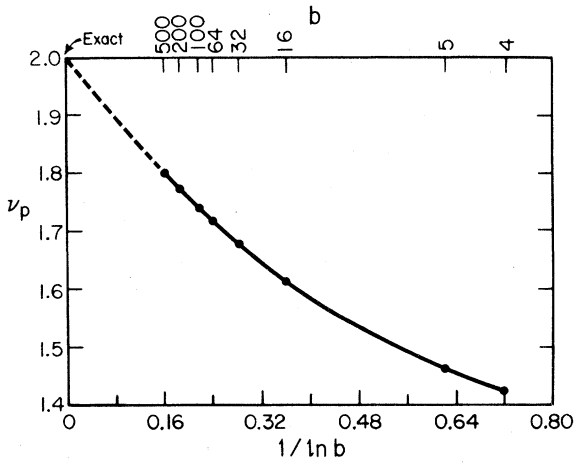

FIG. 16. Connectedness length exponent ν_p for the linear chain with nearest- and next-nearest-neighbor bonds $(L=2)$ is plotted against $1/\ln b$, with b the rescaling length. This entire curve was obtained from Eq. (A8) with $b\equiv l/L=\frac{1}{2}l$. We note that the exact result for ν_p is obtained in the limit of $b\to\infty$. To indicate how the extrapolation methods discussed in Sec. V may be used, we have drawn in points at the same values of b used in the $d=2$ calculations, up to $b=500$. The dashed portion of the curve may be thought of as the extrapolation to $b=\infty$.

where the final term on the right-hand side of Eq. (A10) is the number of ways of choosing L sites out of a set of l sites excluding L in a row (which no longer spans). Again $p^*=1$ is a solution. Differentiating Eq. (A10) we find

$$Lq'^{L-1}\frac{dp'}{dp}=L(l-L+1)p^{l-L}q^{L-1}+O(q^L) \ . \tag{A11}$$

Thus

$$\left(\frac{q'}{q}\right)^{L-1}\frac{dp'}{dp}=(l-L+1)p^{l-L}+O(q) \ . \tag{A12}$$

Evaluating this at $p^*=1$ we find [cf. Eq. (A3)]

$$\lambda_p=\left.\frac{dp'}{dp}\right|_{p=1}=(l-L+1)^{1/L} \tag{A13a}$$

and

$$\nu_p(l)=\frac{L\ln l/L}{\ln(l-L+1)} \ . \tag{A13b}$$

Again, for finite cells of size l, $\nu_p(l)$ is only an approximation, but

$$\nu_p\equiv\lim_{l\to\infty}\nu_p(l)=L \tag{A14}$$

is the exact result. In Fig. 16 we illustrate the approach to this limit for $L=2$.

*Preliminary reports of portions of the present work appeared in Refs. 18 and 29.

[1]S. R. Broadbent and J. M. Hammersley, Proc. Cambridge Philos. Soc. 53, 629 (1957); M. F. Sykes and J. W. Essam, J. Math. Phys. 5, 1117 (1964). Much of the mathematical percolation literature is reviewed in J. W. Essam, in *Phase Transitions and Critical Phenomena,* edited by C. Domb and M. S. Green (Academic, London, 1972), Vol. 2, p. 197.

[2]R. J. Elliott, B. R. Heap, D. J. Morgan, and G. S. Rushbrooke, Phys. Rev. Lett. 5, 366 (1960); R. J. Birgeneau, R. A. Cowley, G. Shirane, and H. J. Guggenheim, Phys. Rev. Lett. 37, 940 (1976).

[3]H. Müller-Krumbhaar, Phys. Lett. A 50, 27 (1974); C. Domb and E. Stoll, J. Phys. A 10, 1141 (1977); A. Coniglio, C. R. Nappi, F. Peruggi, and L. Russo, J. Phys. A 10, 205 (1977); A. Coniglio and W. Klein (unpublished).

[4]S. Kirkpatrick, Rev. Mod. Phys. 45, 574 (1973); J. P. Straley, Phys. Rev. B 15, 5733 (1977); D. J. Thouless, in *Proceedings of the Les Houches Summer School on Ill-Condensed Matter* (North-Holland, Amsterdam, to be published).

[5]A. Coniglio, H. E. Stanley, and W. Klein, Phys. Rev. Lett. 42, 518 (1979) and references therein.

[6]P. G. de Gennes and E. Guyon, J. Mec. 17, 403 (1978).

[7]D. Stauffer, Phys. Rep. 54, 1 (1979).

[8]S. Kirkpatrick, in *Proceedings of the Les Houches Summer School on Ill-Condensed Matter* (North-Holland, Amsterdam, to be published).

[9]P. W. Kasteleyn and C. M. Fortuin, J. Phys. Soc. Jpn. Suppl. 26, 11 (1969).

[10]R. B. Potts, Proc. Cambridge Philos. Soc. 48, 106 (1952).

[11]For a broad spectrum of reviews on the renormalization group, see *Phase Transitions and Critical Phenomena,* edited by C. Domb and M. S. Green (Academic, London, 1976), Vol. 6.

[12]A. B. Harris, T. C. Lubensky, W. K. Holcomb, and C. Dasgupta, Phys. Rev. Lett. 35, 327 (1975).

[13]R. G. Priest and T. C. Lubensky, Phys. Rev. B 13, 4159 (1976); D. J. Amit, J. Phys. A 9, 1441 (1976); D. J. Amit, D. J. Wallace, and R. K. P. Zia, Phys. Rev. B 15, 4657 (1977).

[14]C. Dasgupta, Phys. Rev. B 14, 1221 (1976); T. W. Burkhardt and B. W. Southern, J. Phys. A 11, L253 (1978).

[15]A. P. Young and R. B. Stinchcombe, J. Phys. C 8, L535 (1975).

[16]S. Kirkpatrick, Phys. Rev. B 15, 1533 (1977).

[17]A. A. Migdal, Zh. Eksp. Teor. Fiz. 69, 810, 1457 (1975).

[18]P. J. Reynolds, W. Klein, and H. E. Stanley, J. Phys. C 10, L167 (1977).

[19]R. B. Griffiths, J. Math. Phys. 8, 484 (1967).

[20]L. G. Marland and R. P. Stinchcombe, J. Phys. C 10, 2223 (1977).

[21]L. G. Marland, J. Phys. C 11, L617 (1978).

[22]Y. Yuge and C. Murase, J. Phys. A 11, L83 (1978); and Y. Yuge, Phys. Rev. B 18, 1514 (1978).

[23]H. Kunz and B. Payandeh, Phys. Rev. B 20, 1285 (1979).

[24]C. Tsallis and G. Schwachheim, J. Phys. C 12, 9 (1979).

[25]B. Shapiro, J. Phys. C 11, L863 (1978).

[26]J. Bernasconi, Phys. Rev. B 18, 2185 (1978).

[27]H. Nakanishi and P. J. Reynolds, Phys. Lett. A 71, 252 (1979); and B. Shapiro, J. Phys. C 12, 3185 (1979).

[28]W. Kinzel, Z. Phys. B 34, 79 (1979).

[29]P. J. Reynolds, H. E. Stanley, and W. Klein, J. Phys. A 11, L199 (1978).

[30]A. C. N. de Magalhães, C. Tsallis, and G. Schwachheim (unpublished).

[31]M. P. M. den Nijs, J. Phys. A 12, 1857 (1979); see also B. Nienhuis, A. N. Berker, E. K. Riedel and M. Schick, Phys. Rev. Lett. 43, 737 (1979).

[32]W. Klein, H. E. Stanley, P. J. Reynolds, and A. Coniglio, Phys. Rev. Lett. 41, 1145 (1978).

[33]W. Klein, H. E. Stanley, S. Redner, and P. J. Reynolds, J. Phys. A 11, L17 (1978).

[34]A. L. Lewis, Phys. Rev. B 16, 1249 (1977); Z. Friedmăn and J. Felsteiner, Phys. Rev. B 15, 5317 (1977).

[35]P. J. Reynolds, H. E. Stanley, and W. Klein, J. Phys. A 10, L203 (1977), and references therein.

[36]Since at least one h bond is necessary to reach the ghost, we may always write $h' = hR_h(p,h)$. Thus $\lambda_h = dh'/dh\big|_{\substack{p=p^* \\ h=0}} = R_h(p^*,0)$ while the cross derivative $dh'/dp \sim h$, vanishes when evaluated at the fixed point, $h^* = 0$. Likewise, $dp'/dh \sim h$, because at least two ghost bonds are required to span a configuration which cannot be spanned without h bonds. Therefore, the 2×2 matrix of derivatives at the fixed point is diagonal in this basis. Since the equations for h' and p' decouple in this way, $(p-p^*)$ and h are the scaling fields.

[37]Loosely speaking, this is because an occupied cell contains a spanning cluster, which will generally extend beyond the cell, being part of a larger cluster. Upon renormalization, the new occupied "site" will also generally extend. Thus we expect that the major change in the number of clusters arises from the small clusters within or between cells being lost upon renormalization. However, the number of clusters smaller than any given size (e.g., the cell size) is *not* singular, and may in fact be written as a polynomial in p.

[38]B. Widom, J. Chem. Phys. 43, 3892, 3898 (1965); A. Hankey and H. E. Stanley, Phys. Rev. B 6, 3515 (1972).

[39]A. G. Dunn, J. W. Essam, and D. S. Ritchie, J. Phys. C 8, 4219 (1975).

[40]M. A. A. Cox and J. W. Essam, J. Phys. C 9, 3985 (1976).

[41]Implicit for the validity of Eq. (3.5) is that asymptotically $X_I > b^{-(d-1)/2}$ for $p \geq p_c$. We note that we may write $X_I \sim b^{d_f^\dagger}/b^d$, where $b^{d_f^\dagger}$ is the number of sites in the spanning cluster, and thus $d_f^\dagger$ is an effective dimension (see Ref. 42) of the spanning cluster. For $p = p_c$, $d_f^\dagger - d = -\beta_p/\nu_p$ from finite-size scaling. We satisfy the requirement on X_I if $\beta_p/\nu_p < \frac{1}{2}(d-1)$ or $\eta_p < 1$. Intuitively, if $d_f^\dagger$ were too small, clusters would not be sufficiently branched to join at the interfaces. Equation (3.5) predicts that this would occur for $d_f^\dagger < \frac{1}{2}(d+1)$. Imagine, e.g., $d_f^\dagger \simeq 1$. Such a spanning cluster would be essentially one-dimensional, and would intersect at the cell boundary in only a few places. As the cell, and hence the boundary, increases in size, the cluster actually becomes *less* likely to link across the surface. For $p > p_c$, a finite fraction of sites belong to the spanning cluster for all b, and so $X_I \sim$ const, leading to $d_f^\dagger = d$, which again satisfies $X_I > b^{-(d-1)/2}$.

[42]Fractal or effective dimensions for the percolation problem are treated in H. E. Stanley, J. Phys. A 10, L211 (1977);

R. J. Harrison, G. H. Bishop, and G. D. Quinn, J. Stat. Phys. 19, 53 (1978). See also D. Stauffer, Z. Phys. B 25, 391 (1976), and Refs. 7 and 8.

[43]Since our concern is with the linking of spanning clusters *between* cells and the preservation of the connectivity upon renormalization, we do *not* wish to treat each cell as a minilattice with periodic boundary conditions (which for ordinary Monte Carlo calculations would be the better method). Therefore all our rules employ open-boundary conditions.

[44]See J. W. Essam in Ref. 1 for a discussion of matching graphs.

[45]J. Hoshen and R. Kopelman, Phys. Rev. B 14, 3438 (1976).

[46]Other Monte Carlo renormalization groups are treated in S.-K. Ma, Phys. Rev. Lett. 37, 461 (1976); and in R. H. Swendsen, Phys. Rev. Lett. 42, 859 (1979) and unpublished.

[47]The number of Monte Carlo realizations from which each of these curves is derived is listed in Table VII.

[48]W. T. Eadie, D. Drijard, E. E. James, M. Roos, and B. Sadoulet, *Statistical Methods in Experimental Physics* (North-Holland, Amsterdam, 1971).

[49]Friedman and Felsteiner, Ref. 34, used this idea for the Ising model, considering cells of maximum size 729 spins. For percolation we have treated a sequence of cells up to size 250 000 sites. Clearly, if one is to extrapolate from the results of finite-cell PSRG, it is desirable to have cells as large as possible. Recently Kirkpatrick, Ref. 8, has used this large cell PSRG on the bond-percolation problem.

[50]M. E. Fisher, in *Proceedings of the 51st Enrico Fermi Summer School, Varenna, Italy,* edited by M. S. Green (Academic, New York, 1971); A. Sur, J. L. Lebowitz, J. Marro, M. L. Kalos, and S. Kirkpatrick, J. Stat. Phys. 15, 345 (1976).

[51]M. F. Sykes, D. S. Gaunt, and M. Glen, J. Phys. A 9, 97 (1976).

[52]M. Schwartz, Phys. Rev. B 18, 2364 (1978); H. Kunz and B. Souillard, J. Stat. Phys. 19, 77 (1978); G. R. Reich and P. L. Leath, J. Phys. C 11, 1155 (1978); and Ref. 7.

[53]J. Roussenq, J. Clerc, G. Giraud, E. Guyon, and H. Ottavi, J. Phys. (Paris) 37, L99 (1976).

[54]M. E. Levinshtein, B. I. Shklovskii, M. S. Shur, and A. L. Efros, Sov. Phys. JETP 42, 197 (1976).

[55]See also M. Suzuki, Prog. Theor. Phys. 58, 1142 (1977).

[56]See, for example, Table I of H. E. Stanley, J. Phys. A 10, L211 (1977).

[57]D. S. Gaunt and H. Ruskin, J. Phys. A 11, 1369 (1978).

[58]J. Blease, J. W. Essam, and C. M. Place, J. Phys. C 11, 4009 (1978).

[59]D. Stauffer (private communication).

[60]G. Shlifer, W. Klein, P. J. Reynolds, and H. E. Stanley, J. Phys. A 12, L169 (1979).

[61]S. Redner and P. J. Reynolds (unpublished).

[62]C. Domb and C. J. Pearce, J. Phys. A 9, L137 (1976).

[63]R. Zwanzig and J. D. Ramshaw, J. Phys. A 10, 65 (1977).